Neuroimage: Reports 3 (2023) 100171

Contents lists available at ScienceDirect

Neuroimage: Reports

journal homepage: www.sciencedirect.com/journal/neuroimage-reports

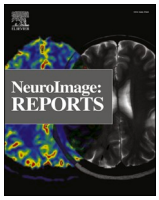

Trait absorption is not reliably associated with brain structure or resting-state functional connectivity

Manesh Girn [a,*], R. Nathan Spreng [a,b,c,d], Daniel S. Margulies [e], Michiel Van Elk [f], Michael Lifshitz [g,h,**]

[a] Department of Neurology and Neurosurgery, Montreal Neurological Institute, McGill University, Montreal, QC, Canada
[b] Departments of Psychiatry and Psychology, McGill University, Montreal, QC, Canada
[c] Douglas Mental Health University Institute, Verdun, QC, Canada
[d] McConnell Brain Imaging Centre, McGill University, Montreal, QC, Canada
[e] Centre National de La Recherche Scientifique (CNRS) and Université de Paris, Paris, France
[f] Department of Psychology, Leiden University, Leiden, Netherlands
[g] Department of Psychiatry, McGill University, Montreal, QC, Canada
[h] Lady Davis Institute for Medical Research, Montreal, QC, Canada

A B S T R A C T

Trait 'absorption' is a psychological construct with a rich history that was initially born from early work on hypnotic suggestibility. Absorption characterizes an individual's tendency to become effortlessly engrossed in the contents of experience, whether in terms of external sensory phenomena or internal imagery and fantasy, and is reliably associated with a constellation of psychological, cognitive, and behavioral traits. Here, we conducted a comprehensive neuroimaging investigation of associations between trait absorption and the brain. In particular, we assessed multivariate relationships between absorption scores and neuroimaging measures of grey matter density, as well as static and dynamic resting-state functional connectivity. We investigated these relationships using partial least squares in a discovery dataset (n = 201) and then attempted to reproduce results in an independent replication dataset (n = 68). Results revealed a lack of significant associations between absorption and grey matter density across both datasets, and a significant association between absorption and static resting-state functional connectivity in the discovery dataset which was not replicated in the replication dataset. Additional control analyses further indicated the lack of a reliable brain-absorption relationship, whereas we found a replicable association between the closely related trait of 'openness to experience' and resting-state functional connectivity. We conclude that absorption is not reliably associated with brain structure or function in the present datasets and discuss factors that may have contributed to this result. This study serves as the first comprehensive and adequately powered investigation of the neural correlates of absorption and motivates future studies to refine the conceptualization of this perplexing trait.

1. Introduction

The personality trait of 'absorption' emerged as a psychological construct from early research seeking to devise a questionnaire measure of hypnotic suggestibility (Lifshitz et al., 2019; Tellegen, 1981). It was originally codified as the 34-item Tellegen Absorption Scale (TAS) in 1974 and a Likert scale version of this scale – referred to as the Modified Tellegen Absorption Scale (MODTAS) – currently serves as the primary measure of this trait (Jamieson, 2005; Tellegen and Atkinson, 1974). 'Absorption' refers to an individual's tendency to become effortlessly engrossed in the contents of experience, whether that experience is externally-directed and stimulus-dependent (i.e., sensory) or internally-directed and endogenously-generated (i.e., imaginative; (Jamieson, 2005; Lifshitz et al., 2019; Tellegen and Atkinson, 1974). Individuals high in absorption appear to be drawn towards episodes of total attentional engagement and a suspension of evaluative and goal-directed thinking. Accordingly, absorption has been described as a tendency to adopt an experiential, as opposed to instrumental, mindset (Tellegen, 1981; Wild et al., 1995). Items of the MODTAS predominantly vary between an emphasis on fantasy and mental imagery on one hand, and responses to external stimuli on the other (Jamieson, 2005; Tellegen and Atkinson, 1974). The scale also includes items pertaining to anomalous sensory and self-related experiences (see Table 1 for examples).

In support of its status as a stable personality trait, studies have found support for the strong test-retest reliability of the absorption as

* Corresponding author.
** Corresponding author. Department of Psychiatry, McGill University, Montreal, QC, Canada.
E-mail addresses: manesh.girn@mail.mcgill.ca (M. Girn), michael.lifshitz@mcgill.ca (M. Lifshitz).

https://doi.org/10.1016/j.ynirp.2023.100171
Received 8 August 2022; Received in revised form 1 February 2023; Accepted 3 April 2023
Available online 8 April 2023

Table 1
Example items from the Modified Tellegen Absorption Scale (Jamieson, 2005; Tellegen and Atkinson, 1974).

When I listen to music, I can get so caught up in it that I don't notice anything else
My thoughts often occur as visual images rather than as words
Sometimes I experience things as if they were doubly real
The crackle and flames of a wood fire stimulate my imagination
I sometimes 'step outside' my usual self and experience a completely different state of being

measured by the TAS ($r = 0.91$, $n = 172$ (Tellegen, 1982); $r = 0.85$, $n = 591$ (Kihlstrom et al., 1989)), and a large body of work has revealed associations between absorption and a rich array of traits and abilities. As detailed in a recent review (Lifshitz et al., 2019) absorption is positively associated with mental imagery ability, hypnotic suggestibility, and fantasy-proneness (Balthazard and Woody, 1992; McConkey et al., 1999; Sutcliffe et al., 1970), creativity (Manmiller et al., 2005), empathy and neural emotional processing (Benning et al., 2015; Wickramasekera, 2007; Wickramasekera and Szlyk, 2003), feelings of self-transcendence (Cardeña and Terhune, 2014), and depersonalization and hallucinatory phenomena (Glicksohn and Barrett, 2003; Perona-Garcelán et al., 2013, 2016). Studies have also reliably found an $r = 0.3$–0.5 correlation between absorption and the personality trait of 'openness to experience' from the canonical 'Big 5' NEO personality inventory (Costa and McCrae, 1989; McCrae and Costa Jr, 1985). Research additionally supports an association between absorption and reports of vivid sensory and spiritual experiences, whether induced by prayer (Lifshitz et al., 2019; Luhrmann and Morgain, 2012; Luhrmann et al., 2010, 2013), a placebo 'god helmet' manipulation (Granqvist et al., 2005; Maij and van Elk, 2018), or psychedelic drugs (Aday et al., 2021; Haijen et al., 2018; Studerus et al., 2012). With respect to psychedelics, trait absorption has also been specifically linked to reports of psychedelic-induced synesthesia (Bresnick and Levin, 2006; Studerus et al., 2012; Terhune et al., 2016) and near-death-like experiences (Timmermann et al., 2018). Of note, one study found that individuals scoring higher in absorption tended to display increased density of serotonin 2A receptors, the primary brain receptor which mediates the effects of serotonergic psychedelic drugs (Ott et al., 2005).

Despite these many associations, however, there has been ongoing debate as to whether the TAS/MODTAS indeed indexes a single psychological factor, and, if so, how exactly that factor should be best interpreted (Terhune and Jamieson, 2021). In support of the former, early work found that the TAS exhibited an internal reliability of $r = 0.88$ ($n = 800$)(Tellegen, 1982). More recently, Jamieson (2005) applied principal component analysis (PCA) to MODTAS responses from 352 subjects and found evidence for a single higher order factor (explaining 26% of total variance), which could additionally be broken down into five intercorrelated sub-factors to explain a total 35% of the variance. Multiple regression analyses also revealed that each sub-factor explained overlapping variance in hypnotic suggestibility – indicating that the associations may have been mediated by a shared factor (Jamieson, 2005). These findings suggest that the items featured in the MODTAS index a shared psychological factor, although confirmatory analyses are required to more reliably ascertain whether this is the case. In contrast to this evidence supportive of reliability, a dearth of construct validation research has led to enduring ambiguity as to what exactly the TAS/MODTAS is measuring. It is unclear, for example, whether absorption should be primarily understood as an increased tendency towards attentional engagement, a particular non-evaluative or non-instrumental cognitive style, or an openness towards anomalous sensory and self-related experiences (Terhune and Jamieson, 2021). More broadly, the jury is still out as to whether absorption should be understood as a single trait or, rather, as a bundle of tendencies and predispositions that tend to hang together for reasons that remain largely unclear (Lifshitz et al., 2019).

Although absorption has a long history and appears to be relevant to a variety of psychological constructs, only one small structural MRI study to date has sought to examine the relationship between absorption and the brain. This highly preliminary study was conducted on a sample of 18 long-term meditators and reported a positive correlation between MODTAS scores and cortical thickness in regions of the frontoparietal control network implicated in attention and cognitive control (Grant et al., 2013). The authors interpreted this finding as suggesting an improved ability for attentional engagement in meditators that score high absorption. This paucity of neural investigations of absorption is likely due to historical limitations in neuroimaging-based individual-differences research, including a lack of sufficiently powered datasets and poor signal-to-noise ratio in relevant assessments (Marek et al., 2022). Critically, however, analytical and technological advances over the past decade (Buckner et al., 2013; Dubois and Adolphs, 2016; Raichle, 2009), combined with the coordinated collection of large-scale neuroimaging brain-behavior datasets (Casey et al., 2018; Mendes et al., 2019; Snoek et al., 2021; Sudlow et al., 2015; Van Essen et al., 2013), have begun to mitigate such challenges and have given rise to a growing field of individual-differences (functional) MRI research (Dubois and Adolphs, 2016). That said, it is important to note that, despite this progress, the field is still plagued by statistical concerns and uncertainty with respect to effect sizes of brain-behavior associations and the corresponding sample sizes required for reliable inferences (Marek et al., 2022).

Neuroimaging investigations examining correlations between mental processes and individual-differences in brain structure and function have relied predominantly on assessments of grey matter density (GMD) and resting-state functional connectivity (RSFC). GMD is computed on the basis of structural MRI and has a history of use in individual-differences research spanning two decades. The most common analytic approach is 'voxel-based morphometry', a volumetric technique that segments the brain into tissue types and estimates local differences in grey matter density on a voxel-wise basis (Ashburner and Friston, 2000). RSFC, on the other hand, emerged as a tool in individual-differences research over the past decade and has become increasingly common only in recent years (Buckner et al., 2013; Dubois and Adolphs, 2016). RSFC is computed on the basis of functional MRI and involves assessing statistical dependencies (e.g., correlations) between the timeseries of spatially distinct voxels or regions in the absence of an explicit task (Buckner et al., 2013). RSFC research has revealed 'intrinsic' networks of preferentially connected regions that are reliable within and between subjects and stable across contexts (Cole et al., 2014; Damoiseaux et al., 2006; Gratton et al., 2018; Yeo et al., 2011; Zuo et al., 2010), and which exhibit overlap with task-evoked coactivation patterns (Cole et al., 2014; Smith et al., 2009) and structural connectivity (Honey et al., 2009; Van Dijk et al., 2010; Vázquez-Rodríguez et al., 2019). RSFC has been used to characterize individual differences in a broad variety of non-neural variables, spanning neuropsychological, cognitive, personality, and demographic measures (Dubois and Adolphs, 2016; Marek et al., 2022; Smith et al., 2015). This literature suggests that individual differences in specific traits may covary with RSFC among brain regions that support the relevant cognitive and behavioral functions (Stevens and Spreng, 2014).

As with many psychological traits, there is reason to think that trait absorption could have a neurocognitive basis (Lifshitz et al., 2019; Ott, 2007). In particular, individual differences in processes related to attention and cognitive control – as mediated by large-scale networks such as the frontoparietal control network (FPCN) and dorsal attention network (DAN) – are strong candidates for mediating variability in this trait. This notion is consistent with the structural MRI study mentioned above (Grant et al., 2013), as well as an early electroencephalographic (EEG) study that found evidence suggestive of heightened attentional flexibility in individuals with high absorption (Davidson et al., 1976). Relevantly, past work has provided evidence that the FPCN can flexibly couple with either the DAN or default network (DN) in a task-dependent manner, in the service of externally-directed (perceptual) or

internally-direction (mnemonic) attention, respectively (Dixon et al., 2018; Spreng et al., 2010). This was found to be underpinned by a bipartite subsystem organization of the FPCN, wherein one subsystem connects preferentially to the DN, and the other to the DAN (Dixon et al., 2018). As such, individual differences in the FPCN's intra-network heterogeneity and its dynamic relationship with the DAN versus the DN may relate to differences in absorption. It has also been suggested that the tendency of high absorption individuals to blur their imagination with incoming sensory input might reflect an increased reliance on top-down predictive signals (i.e., prior expectations) relative to bottom-up sensory prediction errors (Lifshitz et al., 2019). This may be reflected in a stronger connectivity between transmodal (default mode and frontoparietal) and unimodal (visual, somatosensory, and auditory) networks. All in all, the phenomenology of absorption suggests a basis in interactions within and between large-scale brain networks underlying attention, episodic memory/imagination, and sensory processing (Lifshitz et al., 2019; Ott, 2007).

Here we report the first comprehensive investigation of the neural correlates of trait absorption, on the basis of both GMD and RSFC assessments. To do so, we leverage two open-access neuroimaging datasets: the PIOP1 dataset (n = 201) of the Amsterdam Open MRI Collection (Snoek et al., 2021) which serves as our discovery dataset, and the MPI-Leipzig Mind-Brain-Body dataset (n = 68; Mendes et al., 2019) which serves as our replication dataset. With respect to GMD, we hypothesized that higher absorption would be associated with greater GMD in regions comprising the FPCN, consistent with past work (Grant et al., 2013). Both FPCN-specific and whole-brain exploratory GMD analyses were conducted. With respect to RSFC, we hypothesized that higher absorption would be associated with (1) increased RSFC between regions comprising the FPCN and the default network (DN) and DAN, (2) reduced RSFC between FPCN subsystems, (3) increased RSFC between visual and DN regions, (4) reduced differentiation of unimodal and transmodal cortex, (5) decreased modularity, and (6) increased FPCN dynamic network flexibility. Network-specific and whole-brain exploratory RSFC analyses were conducted.

Our results revealed a lack of reliable brain-absorption associations for both GMD and multiple measures of static (time-averaged) and dynamic (time-varying) RSFC. We discuss potential explanations for this lack of reliability, relating both to the specific construct of absorption and to the more general quest to identify neuroimaging signatures of individual differences in cognition and behavior.

2. Methods

2.1. Participants

We used data from two open-access datasets, each containing structural MRI and resting-state fMRI assessments in healthy adult human subjects. The larger of these datasets, the PIOP1 dataset of the Amsterdam Open MRI Collection (Snoek et al., 2021) was used as the discovery sample. 201 subjects (122 women, 79 men; mean age = 22.2, SD = 1.77) from the PIOP1 dataset were included in the present analyses. The MPI-Leipzig Mind-Brain-Body dataset (Mendes et al., 2019) - hereafter referred to as the 'MBB dataset' – was used as a replication sample. 68 subjects (32 women, 36 men; mean age (5-year bins) = 24.5–29.5) from the MBB dataset were included in the present analyses. We selected the larger dataset to be our discovery dataset given that it is more adequately powered.

The putative 'true' non-inflated effect size of multivariate brain-behavior associations has been found to be in the range of r = ~0.30–0.40 (Marek et al., 2022). Our discovery sample (n = 201) provides ≥80% power to detect non-zero correlations r ≥ 0.15 with 95% confidence intervals, whereas our replication sample (n = 68) provides ≥80% power to detect non-zero correlations r ≥ 0.25 with 95% confidence intervals. Both datasets, therefore, provide sufficient statistical power to detect putative multivariate brain-behavior associations involving absorption. Nonetheless, we note that, especially given tendencies toward attenuated effect sizes in out-of-sample replications (Marek et al., 2022), the smaller size of the replication sample does constitute an important limitation in evaluating the true replicability of effects observed in the discovery sample. Another important limitation is that site-related differences pertaining to scanner type and imaging acquisition protocols may represent confounds which may hinder replicability.

2.2. Self-report measures

Self-report measures included in the present analyses are trait Absorption and, for a follow-up analysis (see below), 'openness to experience' from the 'Big 5' personality inventory. Trait Absorption was assessed using the modified (Likert scale) Tellegen Absorption Scale (MODTAS) in both datasets (Jamieson, 2005; Tellegen and Atkinson, 1974). MODTAS scores are hereby referred to as 'absorption scores' for simplicity. Importantly, however, a shortened (15-item) version of the 34-item scale was used in the PIOP1 dataset. This was done due to due to time constraints in data collection and an assumed high correlation between this subset of measures and all of the measures. Items were selected to maintain relative proportions of five putative MODTAS subscales. We empirically tested (in the MBB dataset which assessed all 34 items) whether the mean score produced by the shortened scale correlates strongly with the mean score based on all items. This revealed a correlation of r = 0.96, indicating strong but not perfect correspondence. MODTAS subfactor scores were available for the PIOP1 dataset and were used in secondary analyses. Subfactor (or item-level scores) were not available for the MBB dataset and therefore were not included in the analyses. Trait Openness was assessed in the PIOP1 dataset using the NEO-FFI (Costa and McCrae, 1989), a 60-item version of the NEO inventory, and in the MBB dataset using the NEO-PIR, the full 240-item version of the NEO inventory (Costa Jr and McCrae, 2008).

2.3. Neuroimaging data acquisition

2.3.1. Discovery sample: PIOP1 dataset

Magnetic resonance imaging (MRI) was acquired on a Philips 3T scanner (Philips, Best, Netherlands) equipped with a 32-channel head coil. For each participant a number of scans were recorded over a 60-min scan session. In temporal order, there were faces (fMRI), gender-Stroop (fMRI), T1-weighted scan, emotion matching (fMRI), resting-state (fMRI), phase-difference fieldmap (B0) scan, diffusion-weighted imaging scan, working memory (fMRI), and emotion anticipation (fMRI). Only the T1-weighted and resting-state scans were used in the present analyses.

The high-resolution anatomical (i.e., T1-weighted) image was acquired using a 3D MPRAGE sequence with the following parameters: voxel size = 1.0 mm isotropic, FOV = 188 × 240 × 220 mm, TR = 8500 m, TE = 3.9 m, flip angle = 8°, bandwidth = 191.5 Hz/Px, SENSE acceleration with 2.5 (RL)/2 (FH), duration = 6 min 3 s.

Two resting-state fMRI scans were acquired in axial orientation using T2*-weighted gradient-echo echo planar imaging with multiband acceleration, sensitive to blood oxygen level-dependent (BOLD) contrast. Sequences were as follows for both runs: voxel size = 3 mm isotropic, FOV = 240 × 240 × 118 mm, imaging matrix = 80 × 80, 36 slices with 3 mm thickness, TR = 750 m, TE = 28 ms, flip angle = 60°, bandwidth = 39.5 Hz/Px, multiband acceleration factor = 3, 480 vol, duration = 6 min. Participants were instructed to remain awake with their eyes open and to fixate on a crosshair.

2.3.2. Replication dataset: MPI-leipzig MBB dataset

MRI data was acquired on a Siemens 3T scanner (Magnetom Verio, Siemens Healthcare, Erlangen, Germany) equipped with a 32-channel Siemens head coil at the Day Clinic for Cognitive Neurology, University of Leipzig. For each participant the following scans were obtained:

1) a high-resolution structural scan, 2) four resting-state fMRI scans, 3) two gradient echo fieldmaps and, 4) two pairs of spin echo images with reversed phase encoding direction.

The high-resolution structural image was acquired using a 3D MP2RAGE sequence with the following parameters: voxel size = 1.0 mm isotropic, FOV = 256 × 240 × 176 mm, TR = 5000 m, TE = 2.92 m, TI1 = 700 m, TI2 = 2500 m, flip angle 1 = 4°, flip angle 2 = 5°, bandwidth = 240 Hz/Px, GRAPPA acceleration with iPAT factor 3 (32 reference lines), duration = 8.22 min. From the two images produced by the MP2RAGE sequence at different inversion times, a quantitative T1 map and a uniform T1-weighted image were generated. The latter image is purely T1-weighted, whereas standard T1-weighted image, acquired with the MPRAGE sequence, also contain contributions of proton density and T2*. This difference may influence morphometric assessments and is addressed in *Methods Section 2.5* below.

Four resting-state fMRI scans were acquired in axial orientation using T2*-weighted gradient-echo echo planar imaging with multiband acceleration, sensitive to BOLD contrast. Sequences were identical across the four runs, with the exception of alternating slice orientation and phase-encoding direction, to vary the spatial distribution of distortions and signal loss. Thus, the y-axis was aligned parallel to the AC-PC axis for runs 1 and 2, and parallel to orbitofrontal cortex for runs 2 and 4. The phase-encoding direction was A–P for runs 1 and 3, and P–A for runs 2 and 4. Sequences were set as follows for all four runs: voxel size = 2.3 mm isotropic, FOV = 202 × 202 mm^2, imaging matrix = 88 × 88, 64 slices with 2.3 mm thickness, TR = 1400 m, TE = 39.4 m, flip angle = 69°, echo spacing = 0.67 m, bandwidth = 1776 Hz/Px, partial fourier 7/8, multiband acceleration factor = 4, 657 vol, duration = 15 min 30 s. Participants were instructed to remain awake with their eyes open and to fixate on a crosshair.

2.4. Neuroimaging preprocessing and denoising

A uniform preprocessing and denoising pipeline was applied to both datasets, using a combination of fMRIprep (Esteban et al., 2019) and xcpEngine (Ciric et al., 2018) software packages.

2.4.1. Anatomical data preprocessing

Anatomical data preprocessing was conducted with the fMRIprep software (Esteban et al., 2019). The following description has been copied from this software to best facilitate reproducibility. The T1-weighted (T1w) image was corrected for intensity non-uniformity (INU) with 'N4BiasFieldCorrection', distributed with ANTs 2.2.0 (Avants et al., 2009), and used as T1w-reference throughout the workflow. The T1w-reference was then skull-stripped with a Nipype implementation of the 'antsBrainExtraction.sh' workflow (from ANTs), using OASIS30ANTs as target template. Brain tissue segmentation of cerebrospinal fluid (CSF), white-matter (WM) and grey-matter (GM) was performed on the brain-extracted T1w using fsl fast (Jenkinson et al., 2012).

Brain surfaces were reconstructed using FreeSurfer recon-all (Fischl, 2012) and the brain mask estimated previously was refined with a custom variation of the method to reconcile ANTs-derived and FreeSurfer-derived segmentations of the cortical grey-matter.

Volume-based spatial normalization to one standard space (MNI152NLin2009cAsym) was performed through nonlinear registration with 'antsRegistration' (ANTs 2.2.0), using brain-extracted versions of both T1w reference and the T1w template.

2.4.2. Functional data preprocessing

Functional data preprocessing was conducted with the fMRIprep software (Esteban et al., 2019). For each of the BOLD runs found per subject, the following preprocessing steps were performed: First, a reference volume and its skull-stripped version were generated using a custom methodology of fMRIPrep. The BOLD reference was then co-registered to the T1w reference using bbregister (FreeSurfer (Fischl, 2012);) which implements boundary-based registration. Co-registration was configured with six degrees of freedom. Head-motion parameters with respect to the BOLD reference (transformation matrices, and six corresponding rotation and translation parameters) are estimated before any spatiotemporal filtering using McFlirt (FSL (Jenkinson et al., 2012);). BOLD runs were slice-time corrected using '3dTshift' from AFNI (Cox, 1996). The BOLD time-series were resampled onto their original, native space by applying the transforms to correct for head-motion.

The BOLD time-series were resampled into standard space, generating a preprocessed BOLD run in MNI152NLin2009cAsym space. First, a reference volume and its skull-stripped version were generated using a custom methodology of fMRIPrep Several confounding time-series were calculated based on the preprocessed BOLD: framewise displacement (FD), DVARS (Power et al., 2012) and three region-wise global signals. FD and DVARS are calculated for each functional run, both using their implementations in Nipype. The three global signals are extracted within the CSF, the WM, and the whole-brain masks.

Additionally, a set of physiological regressors were extracted to allow for component-based noise correction (aCompCor (Behzadi et al., 2007);). Principal components were estimated after high-pass filtering the preprocessed BOLD time-series (using a discrete cosine filter with 128s cut-off). aCompCor components were calculated separately within the WM and CSF masks. For each CompCor decomposition, the *k* components with the largest singular values are retained, such that the retained components' time series are sufficient to explain 50 percent of variance across each nuisance mask (CSF and WM). The remaining components are dropped from consideration.

2.4.3. Functional data denoising

Functional data denoising was conducted with xcpEngine. The '36P + SCRUB' pipeline of xcpEngine (https://xcpengine.readthedocs.io/overview.html) was applied to the fMRIprep preprocessed data in both datasets. This stringent pipeline is consistent with the motion artefact removal pipeline originally proposed by Power et al. (2012, 2014). The following denoising steps were applied: demeaning and detrending, nuisance regression, bandpass filtering (0.01–0.08 Hz) and scrubbing (FD > 0.5 mm). Scans with ≥15% of volumes removed (i.e., interpolated) due to scrubbing were excluded from analyses. Nuisance regressors included 6 motion alignment parameters (R) and their derivatives and expansions (R^2 R_{t-1} R^2_{t-1} R_{t-2} R^2_{t-2}) for a total of 36 motion regressors, as well as mean CSF signal as computed within an eroded mask and its derivative, mean WM signal as computed within an eroded mask and its derivative, and the whole-brain global signal and its derivative. The decision to include global signal regression, a controversial denoising technique (Murphy and Fox, 2017), was motivated by recent work suggesting that it may improve sensitivity to brain-behavior associations (Li et al., 2019). Functional data were not smoothed, given that the data were parcellated (which implicitly 'smooths' the data by averaging across voxels) prior to analyses.

2.5. Voxel-based morphometry analyses

2.5.1. GMD calculation

GMD was calculated from the individual-subject T1-weighted images of each dataset using voxel-based morphometry (VBM) as implemented in CAT12, a SPM12 add-on (Ashburner and Friston, 2000; Gaser and Dahnke, 2016). Raw T1-weighted images were first spatially normalized to a high-resolution stereotactic space using the DARTEL template and then underwent automated segmentation into grey matter, white matter, and cerebrospinal fluid (CSF). CAT12 uses a tissue probability map (TPM) prior to skull strip the data and initialize the segmentation, and segmentation is conducted using a hypothesis-free adaptive maximum *a posteriori* (AMAP) segmentation approach (Gaser and Dahnke, 2016). This approach estimates the amount of brain tissue type within each voxel and allows for the control of partial volume effects. We visually inspected the resulting grey matter maps to ensure consistency in

orientation across subjects. Once this was confirmed, the homogeneity of the total sample (comprising both datasets) was evaluated in order to identify outliers. Homogeneity was determined to be high across both datasets with average inter-subject spatial correlations ranging from $r =$ 0.88–0.90. Prior to analysis, total intracranial volume was regressed from the grey matter maps to more reliably extract individual differences in relative grey matter proportions, and the regressed grey matter maps were then smoothed with an 8 mm Gaussian kernel prior to being used as input to the partial least squares correlation (PLSC) analyses (described below in *Section 2.8*).

It was noted above that the Leipzig used a MP2RAGE sequence which removes the influence of proton density and T2* from the T1-weighted image, as compared to the more common MPRAGE sequence which does not do this. We found that this resulted in stronger image quality (IQR) ratings as output by SPM12 in the MBB dataset relative to the PIOP1 dataset (Leipzig range = 1.8–2; PIOP range = ~2–3), where lower values indicate stronger quality. However, as mentioned, tests of homogeneity indicate that the subjects of the MBB dataset were not outliers with respect to the PIOP1 dataset.

2.6. Static resting-state functional connectivity (sRSFC) analyses

2.6.1. sRSFC calculation

The denoised resting-state fMRI voxel-wise timeseries data were parcellated into 451 regions as follows: 400 cortical regions following Schaefer et al. (2017), 32 subcortical regions following (Tian et al., 2020), 17 cerebellar regions following (Buckner et al., 2011), and two regions comprising the bilateral claustrum (Krimmel et al., 2019). Importantly, the timeseries of bilateral putamen and insula parcels located spatially adjacent to the claustrum were regressed from the bilateral claustrum timecourses, following past work indicating that this significantly attenuates the partial volume effects which typically plague this region (Krimmel et al., 2019).

RSFC was computed as the product-moment correlation coefficient between all parcels, then transformed using Fisher's *r*-to-*z* transform, resulting in a 451 × 451 RSFC matrix for each subject. Cortical nodes were organized according to the Yeo et al. (2011) 17 network parcellation for the calculation of network-specific effects and for visualization.

2.6.2. Modularity

Modularity is a measure derived from the subfield of mathematics referred to as graph theory. The application of graph theory to neuroimaging data formalizes the brain as a network of nodes (e.g., brain regions) which are connected by edges/links (e.g., functional correlations, white matter pathways (Bassett and Sporns, 2017; Rubinov and Sporns, 2010);). This formalization enables the quantification of topological properties associated with the brain's graph (i.e., network) structure. Modularity in particular indexes the decomposability of a given network (in this case, whole-brain functional connectivity) into distinct modules.

Modularity was computed using the Louvain algorithm (Blondel et al., 2008) implemented with the Network Community Toolbox (http://commdetect.weebly.com/). This algorithm finds modular partitions of the graph (synonymous with network) which optimize the modularity value, Q, by grouping nodes into non-overlapping (sub) networks that maximize intra-modular and minimize inter-modular connections (Newman, 2004). The modularity value Q for a given modular partition is computed as follows:

$$Q = \frac{1}{l}\sum_{i,j\in N}\left[w_{ij} - \frac{k_i k_j}{l}\right]\delta_{m_i m j}$$

where w is the edge weight (i.e., functional connectivity value) between nodes i and j, l^{w} is the sum of all weights in the graph, k_{i} is the weighted degree (edge weight summed across all edges) of node i, and m_{i} is a module containing node i. $\delta_{m_i m j} = 1$ if nodes i and j belong to the same module, and $= 0$ otherwise. The Q value for a given partition therefore quantifies the strength of within-module edges relative to the strength of between-module edges, or, in other words, the extent to which distinct modules can be delineated in the data. This algorithm has a single free parameter, gamma (γ), which controls how many modules will be detected. We kept this at the default value of 1. The Louvain algorithm was run iteratively 100 times on each individual-subject 451 × 451 RSFC matrix and the average Q value across these runs was used. Given that negative values are not interpretable after applying global signal regression, RSFC matrices were thresholded to include only positive values prior to being input to the modularity algorithm. Associations between subject-wise Q values and absorption were assessed.

2.6.3. Gradient-mapping

Gradient-mapping is a burgeoning approach to characterizing brain functional organization which, instead of parcellating the brain into functionally homogenous brain regions, characterizes the brain as the superposition of continuous axes (i.e., gradients) of feature variation (Haak et al., 2018; Huntenburg et al., 2018; Margulies et al., 2016; Smallwood et al., 2021). A variety of structural, anatomical, molecular, and genetic features have been found to vary in principled and convergent ways across the cortex and gradient-mapping has been fruitfully used to characterize brain organization in diverse contexts (Dong et al., 2021; Girn et al., 2021; Hong et al., 2019; Paquola et al., 2019; Setton et al., 2021; Sydnor et al., 2021). Here, we computed cortical gradients on RSFC data following the pipeline of (Margulies et al., 2016).

Cortical gradients were computed using a diffusion map embedding algorithm, as implemented using the BrainSpace toolbox (https://github.com/MICA-MNI/BrainSpace (de Wael et al., 2020);) in MATLAB. Diffusion map embedding was applied to individual-subject 400 × 400 RSFC matrices (i.e., including cortical parcels only). As has been done previously (e.g., Hong et al., 2019; Margulies et al., 2016), RSFC matrices were z-transformed and thresholded row-wise at 90% sparsity in order to retain only the strongest connections. Cosine similarity was then computed on the thresholded z-matrix in order to generate a similarity matrix which captures the similarity in whole-brain connectivity patterns between vertices. This similarity matrix is required as input to the diffusion map embedding algorithm. The use of cosine similarity as the similarity metric of choice is consistent with past work using this approach (Hong et al., 2019; Margulies et al., 2016; Paquola et al., 2020) which have consistently found that it reveals biologically-relevant axes of cortical organization.

Diffusion map embedding (Coifman et al., 2005), a non-linear manifold learning technique from the family of graph Laplacians, was applied to similarity matrices in order to identify gradient components at the individual subject level. The technique estimates a low-dimensional set of embedding components (gradients) from a high-dimensional similarity matrix, where each embedding represents a dimension of covariance in RSFC pattern similarity. Diffusion map embedding notably allows for the influence of both global and local relationships between data points in the estimation of the embedding space.

Euclidean distance between two points in the embedding space is equivalent to the diffusion distance between probability distributions centered at those points (hence the name of the algorithm), which is equivalent to RSFC pattern similarity. Thus, a given region's gradient score for a given gradient axis represents that region's position in a continuous pattern of in RSFC pattern (dis)similarity between two axis extremes. In other words, greater positive values in a gradient represent greater RSFC similarity to the positive extreme, whereas lower negative values represent greater RSFC similarity to the negative extreme.

Following past work (Bethlehem et al., 2020, de Wael et al., 2020; Hong et al., 2019), iterative Procrustes rotation was performed to align individual-subject embedding (gradient) components to an all-subjects

group average embedding component template. The rotation was applied with 10 iterations, wherein the first iteration aligns all subjects to the template, and subsequent iterations align subjects to the mean of all subjects from the previous iteration. This iterative rotation ensures that gradient axes are matched across subjects and faithful to the data structure. Region-wise gradient values for the first three gradients (explaining the most variance) from this approach were used as input to PLSC analyses examining associations with absorption.

2.7. Dynamic resting-state functional connectivity (dRSFC) analyses

2.7.1. dRSFC calculation

Dynamic RSFC was computed using a sliding-window RSFC approach (Lurie et al., 2018). In particular, RSFC matrices were computed for 45-s Gaussian-tapered sliding windows in each dataset – consistent with past work using this approach (Daws et al., 2022; Lurie et al., 2018). Results for 60-s and 75-s windows are reported in the Supplementary Information. Tapered windows were used as past work has indicated they increase sensitivity to differences between adjacent windows by emphasizing center timepoints (Allen et al., 2014; Leonardi & Van De Ville, 2015). Each window was slid for the number of timepoints equivalent to 1/3 of the window length overlapping, consistent with past work (Cui et al., 2021; Daws et al., 2022) and to reduce computational time-intensiveness.

2.7.2. Network flexibility

Network flexibility is a measure of the number of times a given region changes its network affiliation over the course of a given scan. This metric has been used to characterize differences in relation to development (Yin et al., 2020), learning and cognition (Bassett et al., 2011; Braun et al., 2015), and psychopathology (Braun et al., 2016; Daws et al., 2022; Yin et al., 2022).

Network flexibility was computed using a multilayer modularity algorithm (Bassett et al., 2011; Mucha et al., 2010). Multilayer modularity, Q_{ML}, was estimated 100 times from each 451 × 451 x W matrix as follows:

$$Q_{ML} = \frac{1}{2\mu} \sum_{ijlr} \left[\left(A_{ijl} - \gamma_l \frac{k_{il} k_{jl}}{2m_l} \right) \delta_{lr} + \delta_{ij} \omega_{jlr} \right] \delta(c_{il}, c_{jr}), \quad (3)$$

where $\mu = \frac{1}{2} \sum A_{ijl}$ is the total RSFC of the multilayer network, and $m_l = \frac{1}{2} \sum_{ij} A_{ijl}$ is the total RSFC of layer l, A_{ijl} is the RSFC between region i and j at layer l, $\frac{k_{il} k_{jl}}{2m_l}$ is the expected null RSFC at layer l. The two free γ and ω structural and temporal resolution parameters control the number of modules detected and the strength of inter-layer connections, respectively. Primary analyses were conducted with both parameters set to 1, following past work (e.g., Bassett et al., 2011; Daws et al., 2022). To examine whether effect sizes exhibit any dependencies on γ and ω values, values of 0.6–1.4 in increments of 0.2 were also explored for both parameters.

The multilayer modularity estimation generates a matrix consisting of modular assignments for each region at each layer (i.e., window). Network flexibility is computed on this matrix as the number of times a region changes its modular affiliation across windows, as a proportion of the maximum number of potential changes:

$$f_i = 1 - \frac{1}{L-1} \sum_{l}^{L-1} \delta(c_{il}, c_{jl+1}),$$

Where L is the total number of layers (i.e., windows). Network flexibility scores close to 0 represent regions whose modular affiliation is stable across time, whereas scores close to 1 represent regions whose modular affiliation dynamically changes over time.

2.8. Partial least squares correlation (PLSC)

PLSC, a data-driven multivariate statistical technique, was performed for each neural measure to assess its relationship with absorption (McIntosh and Lobaugh, 2004). This approach was selected because it allows for inferences on multivariate brain-behavior relationships without running into concerns with respect to multiple comparison correction. Past work suggests that it affords strong sensitivity to detect individual and group differences (McIntosh and Mišić, 2013).

PLSC takes as input two variable sets **X** and **Y** and identifies linear combinations of each which maximally covary with each other across participants. In the present context, **X** represents a given neural measure and **Y** represents absorption scores. As such, PLSC, as run in this study, outputs latent variables (LVs) which represent covariance-maximized groupings of neural variables (e.g., voxel-wise grey matter density or interregional functional connectivity) and absorption.

A separate PLSC analysis was computed for each measure to assess its relationship with absorption. The**X** and **Y** matrix for each analysis was centered and normalized across participants. Singular value decomposition of the cross-correlation matrix **X'Y** yields several mutually-orthogonal LVs, each composed of three elements: (i) a left singular vector, containing weights the neural measure; (ii) a right singular vector, containing a weight for absorption; and (iii) a scalar singular value. Squared singular values reflect effect size: they are proportional to the covariance between brain and behavior that is accounted for by each latent variable. The number of latent variables is equal to the rank of **X'Y**; in the present case, this is 1 for analyses with absorption total and 5 for analyses in the PIOP1 dataset which included the 5 absorption subscales.

The significance and reliability of each LV were evaluated using permutation testing and bootstrap resampling, respectively. We assessed the significance of the neural pattern captured by a given LV using permutation tests to determine how different the results are from chance. To do this, 500 permutation tests were computed in which the order of the rows of one of the data matrices (**X**) was randomly permuted. Columns of each permuted matrix are then correlated with the behavioral matrix **Y** and the correlation matrix is subjected to singular value decomposition as described above. This process generates a distribution of singular values under the null hypothesis that there is no relationship between brain and behavior. The significance of the LV is estimated by computing the proportion of times the permuted singular values (covariance explained) is higher than the observed singular values (significance thresholded at $P < 0.05$).

To assess the reliability of weights for individual neural variables (e.g., individual voxels or region pairs) and absorptions, we used bootstrap resampling. The rows of both data matrices (**X** and **Y**) were sampled with replacement and a resampled correlation matrix (**X'Y**) was re-computed. The matrix was subjected to singular value decomposition and the process was repeated 500 times to estimate a sampling distribution for each singular vector (i.e., brain and behavior) weight. To identify neural variables and behaviors that (a) make a large contribution to the overall multivariate pattern and (b) are relatively insensitive to bootstrap resampling, we calculated the ratio between each weight and its bootstrap-estimated standard error. The resulting 'bootstrap ratios' (BSRs) are large for neural variables/behaviors that have large weights and narrow confidence intervals. If the sampling distribution is approximately unit normal, BSRs are equivalent to z-scores. Brain network connections were considered reliable if the absolute value of the BSR >2 (approximately P < 0.05) and were visualized using BrainNet Viewer (Xia et al., 2013).

To account for potential confounds, multiple regression analysis was performed on the association between brainscores and absorption, controlling for sex and age. Brainscores are mathematically expressed as the dot product of the GMD voxel or RSFC edge value in each participant's normalized segmented image or RSFC matrix, and the corresponding salience (i.e., weight) in the pattern derived from the PLSC

group result. Brainscores (subject-level scalars) reflect the degree to which the singular pattern was manifest in a given participant's data. Note that this post-hoc analysis was computed on the brainscores of significant LVs output by the PLSC analyses only.

For the analysis of interregional RSFC, we evaluated network-level contributions to individual differences in absorption. We used a label permuting approach following past work (Shafiei et al., 2019), which determines whether network-specific associations are independent of network size or spatial contiguity. To quantify the network-level contributions to the connectivity pattern identified by the PLSC analysis, we first separated the PLSC BSR matrices into two separate matrices, reflecting positive and negative PLSC weights, respectively. The nodes of the graph represent the 451 brain regions defined by the parcellation scheme, and the edges represent the BSR weight for each pairwise connection. The matrices were thresholded such that BSRs with an absolute value less than 2 were set to 0, which is equivalent to $p < 0.05$ as described above. Positive BSRs greater than 2 were set to 1, and negative BSRs less than −2 were set to −1. The network-level functional connectivity contributions were quantified by averaging the weights of all connections in a given network, thus generating a 17 × 17 matrix. Next, permutation testing was applied on the full thresholded matrix by randomly re-ordering the network labels (preserving the number of nodes originally assigned to each network) and re-calculating the network means 1000 times to build a sampling distribution under the null that network assignment does not contribute to the connectivity pattern. The significance of the pairwise connections of the original 17 × 17 matrix was determined by estimating the proportion of times the values of the sampling distribution were greater than or equal to the original value.

2.9. Out-of-sample replication

To assess the replicability of PLSC neural weights derived from the discovery (PIOP1) dataset in the replication (MBB) dataset, we conducted a BSR-based direct replication. In particular, for results which reached statistical significance in the PIOP1 dataset, we computed the dot product between the neural BSR pattern from the PIOP significant result and the corresponding Leipzig neural input matrix, and then examined the correlation between the resulting values (i.e., one value per Leipzig subject representing the degree to which its input matrix exhibits the LV pattern) and absorption in the MBB dataset.

3. Results

3.1. Self-report results

Descriptive statistics were conducted on the self-report data to assess their reliability and suitability for a linear decomposition method such as PLSC. First, histograms were created for absorption scores in each dataset to determine whether they are approximately normally distributed. This was indeed confirmed (Supplementary Fig. 1). Second, we computed the Cronbach's alpha of absorption assessments for each dataset. This revealed high alpha values (PIOP1 alpha = 0.87, Leipzig alpha = 0.94), indicating strong internal consistency.

Past research has indicated that absorption exhibits a 0.3–0.5 correlation with trait openness to experience (McCrae, 1993), a reliable personality trait from the canonical NEO 'Big Five' personality assessment (Costa Jr and McCrae, 2008; McCrae, 1993). We therefore also assessed associations between absorption and openness as an indirect evaluation of construct validity. Absorption in both datasets exhibited a moderate and statistically significant correlation with openness (PIOP1, $r = 0.47$, $p < 0.001$; Leipzig, $r = 0.31$, $p = 0.03$), further supporting the reliability of the present absorption assessments.

3.2. Voxel-based morphometry

3.2.1. Discovery analyses

Having established the reliability and suitability of absorption scores in both datasets for linear analyses, we applied PLSC to assess whether absorption is associated with inter-individual differences in voxel-wise grey matter density (GMD). First, we conducted a hypothesis-driven PLSC analysis including only voxels within a FPCN mask (as defined based on Schaefer et al. (2017) ROIs and the Yeo et al., (2011) parcellation). No statistically significant latent variable (LV) was found ($p = 0.89$). Given the availability of absorption subscale measurements in the PIOP1 dataset, we conducted an additional PLSC analysis with the five absorption subscales, rather than absorption total. Again, no statistically significant LV was found – although, LV 2 trended towards significance ($p = 0.06$).

Next, we conducted an exploratory whole-brain PLSC between GMD and absorption total. This revealed no statistically significant LV ($p = 0.61$). For comprehensiveness, we also assessed whole-brain GMD-absorption correlations using a standard mass univariate GLM approach as implemented in SPM12, controlling for age, sex, and total intracranial volume. This revealed no significant clusters at $p_{FWE} < 0.05$. A PLSC analysis between whole-brain GMD and absorption subscales revealed one statistically significant LV (LV 2, $p = 0.042$, 19.05% covariance explained; Fig. 1).

This LV indicates a pattern of covariance between GMD and absorption which differentiates the absorption subscales of imagination and synesthesia (positive) from extrasensory perception and altered state of consciousness (negative). Neural results predominantly implicate salience and limbic regions including the right anterior cingulate and clusters within the bilateral inferior and middle frontal gyrus (positive), and a broad set of clusters predominantly located within lateral parietal and lateral temporal regions comprising the dorsal attention, visual, frontoparietal, and temporal-parietal networks (negative).

3.2.2. Replication analyses

We failed to find a significant association between GMD and absorption total in the discovery (PIOP1) dataset. This null finding was replicated in the MBB dataset, wherein PLSC analyses similarly did not find a significant latent variable linking GMD and absorption ($p = 0.72$). Given that the LV from the PIOP1 absorption subscale analysis represents an axis of covariance that pertains to a dissociation between absorption subscales and, given that it only minimally correlated with absorption total ($r = 0.07$), a true replication in the MBB dataset (for which absorption subscales are not available) was not possible. Nonetheless, for comprehensiveness, we conducted a direct replication in which we computed brainscores from the PIOP-derived LV 2 BSR weights and the Leipzig individual-subject GMD matrices and assessed their correlation (controlling for sex effects) with absorption total in the MBB dataset. This revealed a correlation of $r = -0.02$, indicating a lack of an association between this PIOP1-derived pattern of covariance and absorption total in the MBB dataset.

3.3. Static resting state functional connectivity

3.3.1. Interregional RSFC

3.3.1.1. Discovery analyses. We hypothesized that higher absorption would be associated with (1) increased RSFC between regions comprising the FPCN and each of the default network (DN) and DAN, (2) reduced RSFC between FPCN subsystems, and (3) increased RSFC between visual and DN regions. Accordingly, two hypothesis-driven PLSC analyses were conducted: one examining multivariate associations between the regions comprising the FPCN, DN, and DAN and absorption, and another between the regions comprising the DN and visual network

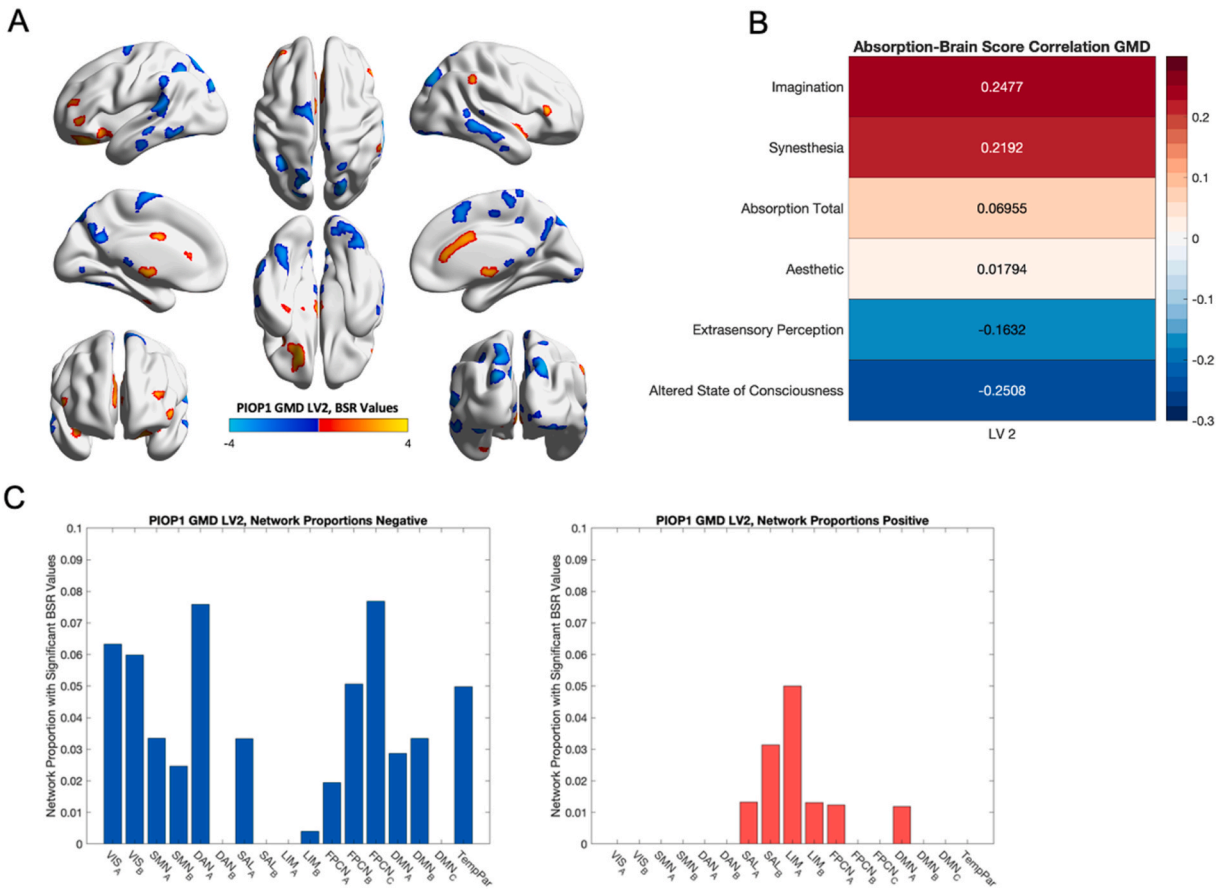

Fig. 1. Results for latent variable 2 ($p < 0.05$) in the PIOP1 discovery dataset, representing a multivariate association between absorption and grey matter density. (A) Voxel-wise BSR values, thresholded at abs(BSR≥2), indicating the most reliable neural weightings of latent variable 2 (B) Correlations between latent variable 2 subject-level brainscores and absorption scores, controlling for age and sex. Note: absorption total was not included in the original model given the redundancy (C) The proportions of each of the 17 large-scale networks identified by (Yeo et al., 2011) exhibiting a significantly reliable BSR value, based on the significant voxels shown in (A). All displayed network level results were significant at $p < 0.05$ via network permutation testing.

and absorption. Network were defined based on the Schaefer-Yeo 17 network parcellation (Schaefer et al., 2017; Yeo et al., 2011). The former revealed a trending but non-significant effect ($p = 0.076$) and the latter revealed a non-significant effect ($p = 0.19$).

We next conducted an exploratory analysis evaluating whether whole-brain interregional RSFC (400 × 400; Schaefer et al., 2017) is associated with absorption. PLSC results with the PIOP1 dataset revealed one statistically significant LV for absorption ($p = 0.01$, 58.19% covariance explained; Fig. 2). No additional latent variables were found when computing the model with the five absorption subscales.

This LV represents a set of interregional RSFC connections that jointly covary with absorption scores. Post-hoc correlations with absorption subscales revealed that all subscales were strongly positively associated with this effect, with the highest correlations being with the 'altered state of consciousness' and 'aesthetic' subscales. Neural results implicate several inter-network relationships. Notably, increased RSFC between visual-central (i.e., including V1) and attentional networks (DAN and FPCN), alongside decreased RSFC between this network and default and auditory networks, was associated with increased absorption. In addition, increased FC between default network subsystem C (encompassing the medial temporal lobes) and sensorimotor networks was found to be positively associated with absorption. Overall, results indicate that the absorption phenotype is associated with a complex pattern spanning interregional interactions between a variety of networks.

3.3.1.2. Replication analyses. To evaluate the replicability of the result with the PIOP1 dataset, we computed brain connectivity scores from the PIOP1-derived LV 1 BSR weights and the Leipzig individual-subject RSFC matrices and assessed their correlation (controlling for sex effects) with absorption in the MBB dataset. This revealed a correlation of $r = 0.04$ (as compared to $r = 0.77$ in the PIOP1 dataset), indicating a lack of replication at the whole-brain level.

To evaluate replicability at a more fine-grained level, we also computed brain connectivity scores for each of the statistically significant network x network pairs as shown in Fig. 3B. This allowed us to derive correlations (for both datasets) between absorption and the extent to which a given network x network RSFC pattern expresses the pattern found in the corresponding network x network BSR weights from PIOP LV 1. Results are shown in Fig. 3.

Results indicate that the correlations in the Leipzig (replication) dataset are unreliable for the network pairs which exhibited significant correlations in the PIOP1 datasets. This indicates a lack of replication of this result across datasets.

Finally, for comprehensiveness we also computed univariate correlations between network-averaged RSFC (i.e., average RSFC across all connections within and between each network) for each of the 17 networks of Yeo et al. (2011) and absorption for each of PIOP1 and MBB datasets (Supplementary Fig. 2). No overlap between results from each dataset was observed ($p < 0.05$ uncorrected), further confirming the absence of a reliable association between RSFC and absorption in the present datasets.

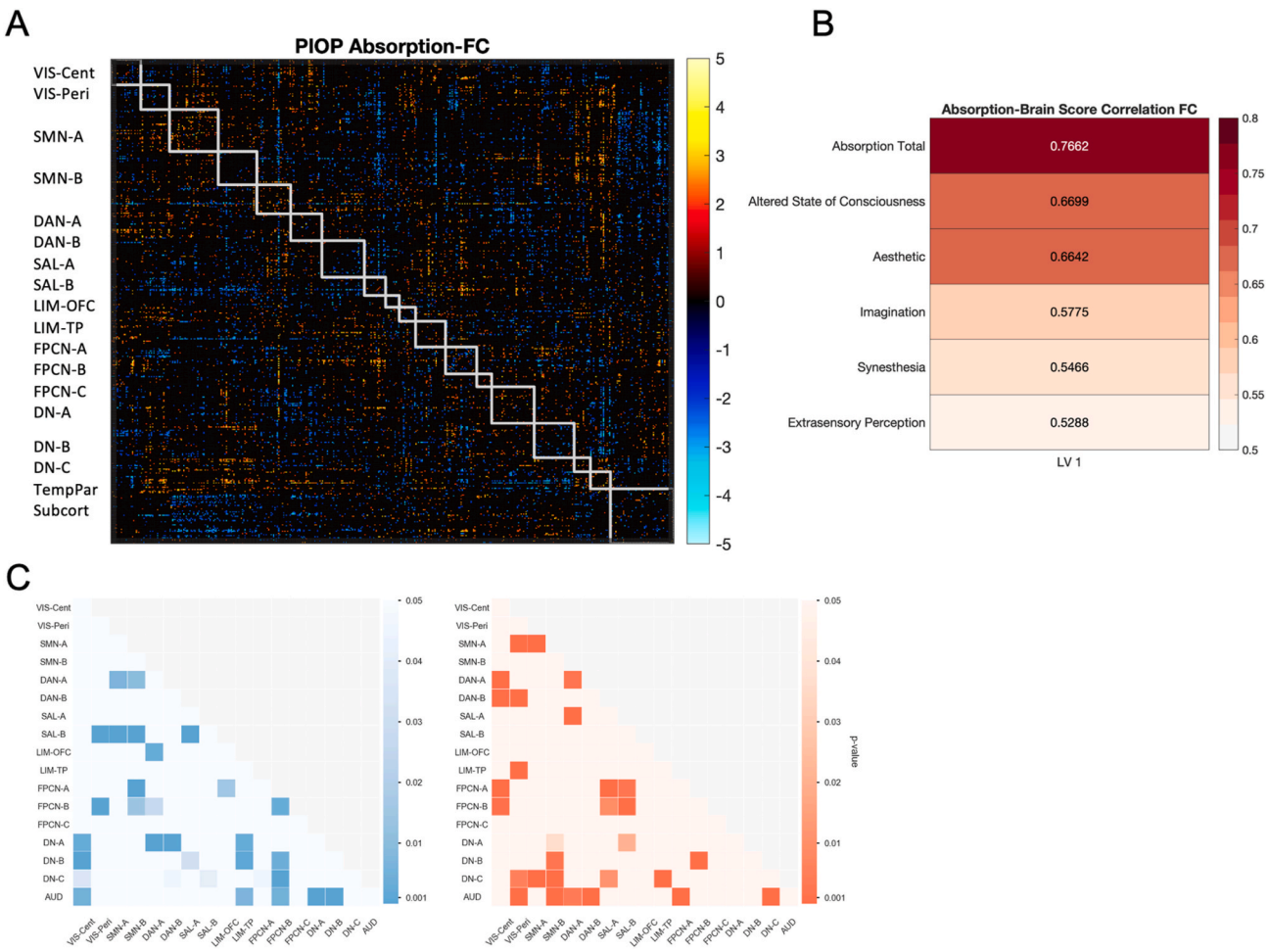

Fig. 2. Results for latent variable 1 ($p < 0.05$) in the PIOP1 discovery dataset, representing a multivariate association between absorption and resting-state functional connectivity (RSFC). Results were computed by a partial least squares analysis on RSFC and absorption subscale scores in the PIOP1 (discovery) dataset. (A) BSR values for interregional RSFC connections, thresholded at abs(BSR≥2), indicating the most reliable neural weightings of latent variable 1. (B) Correlations between latent variable 1 subject-level brainscores and absorption scores, controlling for age and sex. Note: the latent variable was computed using only absorption total and the analysis did not include subscale scores. Post-hoc correlations with each subscale were computed and visualized here for interpretational purposes only. (C) Each of the 17 large-scale networks identified by (Yeo et al., 2011) exhibiting a significantly reliable BSR value at the network level, based on network permutation testing (see *Methods*), separated into negative (left) and positive (right) values.

3.3.2. *Modularity*

We hypothesized that decreased whole-brain network modularity would be positively associated with absorption. Motivation for this hypothesis comes from evidence indicating that a 5-HT2A receptor polymorphism associated with increased expression of this receptor may be associated with higher absorption scores (Ott et al., 2005), combined with findings indicating that 5-HT2A agonist psychedelic drugs acutely and post-acutely decrease modularity (Daws et al., 2022; Tagliazucchi et al., 2016). In addition, the putative phenomenology of absorption (e.g., synesthesia and blurring between sensory and imaginative worlds) suggests decreased neural functional differentiation. However, analyses failed to find a significant association between modularity and absorption ($p = 0.81$).

3.3.3. *Gradient-mapping*

We hypothesized that decreased functional differentiation between high level (i.e., transmodal) and low level (i.e., sensorimotor) cortical regions would be positively associated with absorption. This would be broadly consistent with an increased influence of abstract, mnemonic processes on sensory processes – as seems to be present for individuals high in absorption. We applied 'diffusion map embedding' – a technique that characterizes macroscale axes of functional connectivity similarity and has been fruitfully used to characterize (hierarchical) cortical functional organization in a variety of contexts, in both health and disease (Dong et al., 2021; Girn et al., 2021; Hong et al., 2019; Margulies et al., 2016; Murphy et al., 2018; Setton et al., 2021; Smallwood et al., 2021; Sydnor et al., 2021). This technique revealed macroscale gradients consistent with prior work (Supplementary Fig. 3). Separate PLSC analyses were conducted for each of the first three gradients, assessing their multivariate relationships with absorption. No significant latent variables were found gradient 1 (unimodal sensory to transmodal association) $p = 0.16$, gradient 2 (somatomotor to visual) $p = 0.27$, gradient 3 (executive to non-executive) $p = 0.08$.

3.4. *Dynamic resting state functional connectivity (dRSFC)*

3.4.1. *Network flexibility*

We additionally sought to evaluate whether absorption is captured by *dynamic* RSFC, as opposed to the 'static' time-averaged RSFC upon which the above measures are based. In particular, we used a sliding-window RSFC approach and computed network flexibility, computed as the number of times a given region changes its modular (i.e., network) affiliation across successive windows. We computed this measure across multiple window lengths (45, 60, and 75 s) and multiple values of the γ and ω parameters (see *Methods Section 2.7* above). We hypothesized that greater network flexibility of the FPCN would be associated with higher

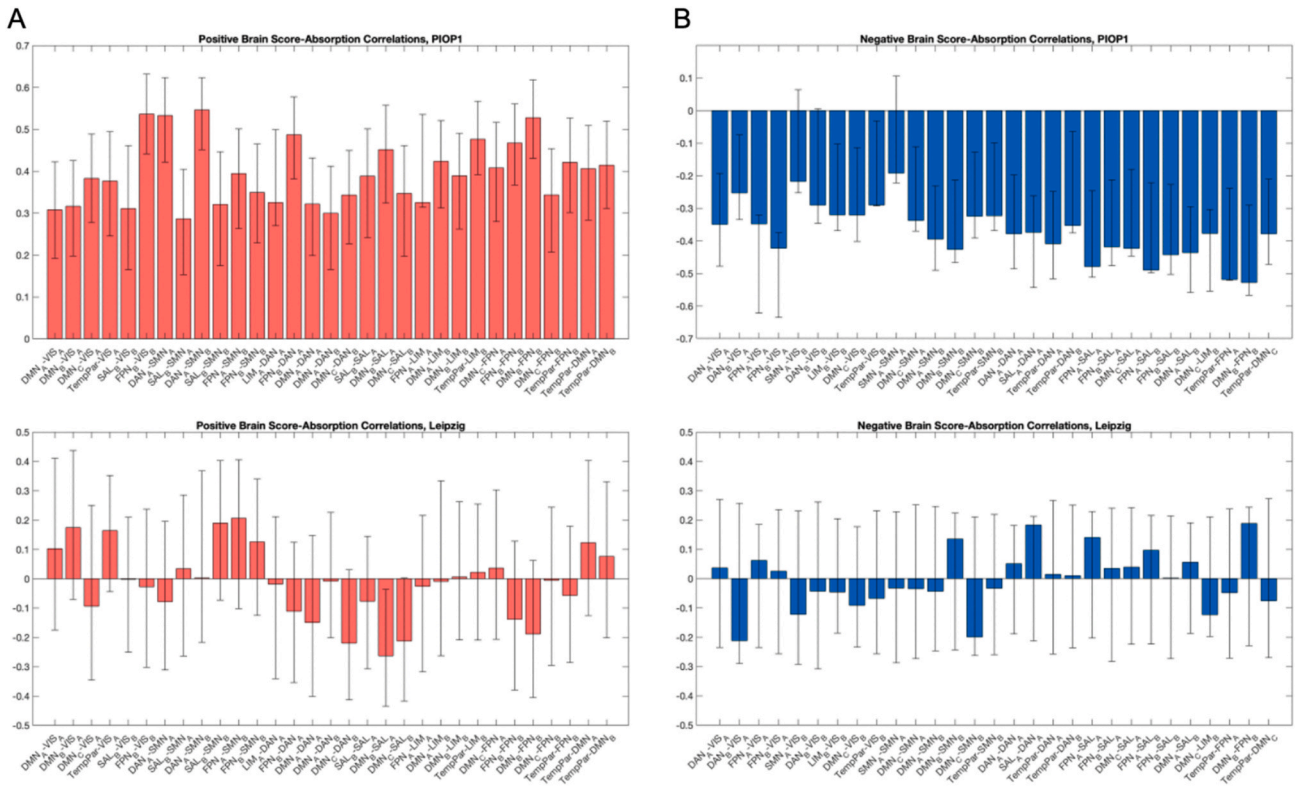

Fig. 3. Direct replication of LV 1 ($p < 0.05$) as found in the PIOP1 dataset, representing an association between whole-brain RSFC and absorption. Bar plots display correlations between network x network BSR values (derived from LV 1 of the PIOP1 dataset) and absorption in both datasets. **(A)** Correlations between network x network pairs which display positive values in PIOP1 LV1 and absorption in each of the PIOP1 (top) and Leipzig (bottom) datasets. **(B)** Correlations between network x network pairs which display negative values in PIOP1 LV1 and absorption in each of the PIOP1 (top) and Leipzig (bottom) datasets.

absorption scores. PLSC analyses evaluating associations between the network flexibility of FPCN nodes and absorption revealed *p* values ranging from 0.26 to 0.83 across parameters and window lengths – indicating no statistically significant LVs. Exploratory whole-brain analyses between network flexibility and absorption similarly revealed no statistically significant LVs ($p = 0.19$ to 0.72).

3.5. Control analysis with openness to experience

Our analyses failed to find a reliable association between absorption and brain structure or resting-state function across the two investigated datasets. To ensure that this was not due to an issue pertaining to the present datasets in general, we also computed associations between GMD and RSFC and the personality trait of openness to experience. As mentioned, openness is a reliable and stable personality trait from the canonical NEO 'Big 5' personality inventory and exhibited a statistically significant correlation with absorption in the present datasets. PLSC analyses with the PIOP1 dataset revealed no significant latent variable for GMD ($p = 0.60$), and one statistically significant latent variable for whole-brain interregional RSFC ($r = 0.78$, $p = 0.02$). Critically, this latter effect was directly replicated in the MBB dataset – albeit with a much smaller effect size ($r = 0.28$, $p = 0.02$; see Supplementary Fig. 4). The successful replication with openness to experience suggests that failures of replication with absorption are likely related to the measure itself, rather than to issues pertaining to scanning acquisition parameters or signal to noise ratio.

4. Discussion

The present study constitutes the first comprehensive assessment of the association between trait absorption and brain structure and function. In particular, PLSC was applied to assess multivariate associations between absorption and GMD along with several measures of both static (time-averaged) and dynamic (time-varying) RSFC. Analyses were conducted on a discovery dataset (n = 201), and an out-of-sample (n = 68) replication was attempted for statistically significant effects. Results revealed no statistically significant association between GMD and absorption in either dataset. Across the multiple measures of static and dynamic RSFC, only whole-brain interregional RSFC was significantly associated with absorption in the discovery dataset ($p < 0.05$) – however, this effect did not replicate in the replication dataset. Additional analyses revealed that univariate assessments of associations between absorption and GMD or interregional RSFC also failed to yield replicable effects. Finally, as an evaluation of the reliability of the datasets themselves, we analyzed brain-behavior associations involving trait openness to experience and found that, in contrast to absorption, this trait was associated with interregional RSFC in a manner that replicated across datasets. This set of results indicates a lack of reliable associations between trait absorption and brain structure or function as measured by neuroimaging.

The lack of reliable brain-absorption associations in the present study can likely be attributed to a combination of two factors: (i) the conceptual and psychometric properties of the construct of absorption itself and (ii) broader concerns related to neuroimaging-based individual-differences research in general. With respect to the former, despite strong internal and test-retest reliability – as well as reliable correlations with other traits and abilities – uncertainty with respect to the construct validity of absorption remain (Terhune and Jamieson, 2021). As mentioned, the TAS/MODTAS features a set of items that are, at first glance, relatively heterogenous – varying between a focus on attentional engagement, visual imagery/fantasy, synesthesia, and anomalous perceptual/self-related experiences. Consistent with this heterogeneity, factor analysis has revealed that trait absorption can be decomposed into a set of interrelated but distinct subfactors, although the exact number of

subfactors has varied across studies (Glicksohn and Barrett, 2003; Jamieson, 2005). The presence of subscale heterogeneity is also supported by the absorption subscale analysis conducted with GMD in the present study, which revealed a dissociation between absorption subscales in their associations with brain structure (see Fig. 1). Given this complex structure, it remains to be established how absorption is to be best interpreted (Terhune and Jamieson, 2021) – or, indeed, whether it is best viewed as a unified psychological construct at all, as opposed to a set of distinct tendencies which have a strong (but imperfect) tendency to co-occur.

Evidence also exists that suggests that absorption scores are highly sensitive to context. For example, one study found that the correlation between absorption and hypnotic suggestibility was significantly higher when absorption was assessed alongside independent measures of mental imagery and imagination – suggesting its sensitivity to contextual priming effects (Barnier and McConkey, 1999). Tellegen himself has also argued that trait absorption likely manifests differently across contexts and individuals, depending on, for example, their personal history, as well as present motivational contexts, social cues, and action possibilities (Tellegen, 1981). Our inability to detect reliable associations between absorption and the brain may be interpreted as further support for an understanding of trait absorption as a heterogenous construct that encompasses a set of interrelated but distinct tendencies that manifest in varying person-specific and context-dependent ways. It may be that associations between absorption and brain structure or function would be amplified if the brain data were acquired in constrained contexts that evoke behaviors associated with absorption (Finn et al., 2017; Greene et al., 2018). Such contexts may include, for example, mental imagery tasks, hypnotic inductions, or naturally absorbing stimuli. Another possibility is that naturalistic movie-viewing paradigms may improve brain-absorption associations, an idea consistent with recent findings that such paradigms are superior to the resting-state for achieving reliable FC-based prediction of cognitive and emotional traits (Finn and Bandettini, 2021).

Our failure to find consistent associations between brain measures and absorption may also be related to a lack of statistical power (Button et al., 2013; Marek et al., 2022; Poldrack et al., 2017). Several investigations have established that underpowered studies are the norm in neuroimaging research (as well as in much of biomedicine) and that, accordingly, the literature is riddled with inflated effect sizes and non-replicable false positives (Button et al., 2013; Ioannidis, 2005, 2008; Marek et al., 2022; Poldrack et al., 2017). Effect size estimates – in this case, correlations between the brain and non-neural measures – can vary widely at small sample sizes. One recent large-scale investigation of neuroimaging-based brain-behavior associations found that the 'true' effect sizes of a variety of univariate correlations was $|r < 0.12|$ (as determined based on a sample of >3000 subjects), and that subsamples of size n = 100 derived from this large sample featured correlations that ranged from approximately $r = -0.3$ to 0.3 within a 95% confidence interval (Marek et al., 2022). Importantly, however, effect sizes were found to be larger ($r = 0.4$ to 0.6, n = ~2000) and more replicable when using multivariate analyses, such as canonical correlation analysis (a technique highly similar to the PLSC approach adopted here; (Marek et al., 2022). In addition, it is critical to note that Marek et al. based their effect size estimates on a very limited set of behavioral measures, some of which exhibit poor reliability and unclear construct validity (DeYoung et al., 2022; Tiego and Fornito, 2022). Therefore, while, at face value, our results appear consistent with previous work in suggesting that the reliable detection of personality differences in brain structure likely requires thousands of subjects, it is essential to note that the reliability of the measures in question is an essential factor. It is very possible that a more refined assessment of absorption that features greater reliability and clear construct validity may yield reliable associations with brain structure at the sample sizes employed in the present study (DeYoung et al., 2022; Tiego and Fornito, 2022).

Indeed, this latter point is supported by our successful replication of a brain-behavior association between interregional RSFC and trait openness to experience ($r = 0.78$ discovery, $r = 0.28$ replication; Supplementary Fig. 4). This finding is consistent with a notable large-scale study (n = 889), which found that among the Big 5 personality traits – openness, conscientiousness, extraversion, agreeableness, and neuroticism – RSFC-based predictions were most reliable for openness (Dubois et al., 2018). We highlight, however, that although a significant correlation was found in the replication dataset, this value was far lower (a difference of $r = -0.50$) than in the discovery dataset – broadly consistent with the attenuated out-of-sample effect sizes found by (Marek et al., 2022). This suggests the likelihood of overfitting in the discovery dataset. Nonetheless, it is notable that the discovery effect size of this association is very similar to the discovery effect size found between interregional RSFC and absorption ($r = 0.77$). As such, we might reasonably expect the out-of-sample effect size of this latter finding to also be in the range of $r \sim = 0.25$. Given that our replication sample (n = 68, four 15-min resting-state scans) is sufficiently powered to detect effects of $r \geq 0.25$ with a 95% confidence interval (see *Methods*), it should, therefore, be of sufficient sensitivity to detect the effect found in the discovery dataset. This further suggests that our null findings may be due to the non-replicability of brain associations with trait absorption in particular, rather than solely due to the use of underpowered datasets.

We failed to find a significant association between GMD and absorption or openness to experience in either dataset, using both PLSC and standard GLM-based univariate approaches. At first glance, this appears at odds with previous neuroimaging studies which have found links between personality and brain structure, including with respect to openness (e.g., Vartanian et al., 2018) and absorption (Grant et al., 2013). However, the present null findings are less surprising when considering that past studies examining GMD-behavior associations have predominantly used small and underpowered (mostly n < 50) samples and have produced effects which rarely replicate (Avinun et al., 2020; Boekel et al., 2015; Genon et al., 2022; Marek et al., 2022; Masouleh et al., 2019). Indeed, in a recent large-scale (n = 1107) GMD-personality study, Avinun et al. (2020) not only failed to replicate past findings with the Big 5 personality traits, but also failed to find any statistically significant associations in their whole-brain exploratory analyses. These findings are therefore also consistent with enduring difficulties linking brain structure to personality, which likely have their basis in a combination of construct-specific (reliability and validity) and statistical-power-related limitations.

In conclusion, our results indicate that absorption is not reliably associated with individual differences in brain structure or function. Using two datasets from independent labs (n = 201 and n = 68), we were unable to find any reliable association between trait absorption scores and a range of neuroimaging measures. It is indeed possible that the true effect size of such associations is much lower than suggested here, and that replication in a larger (i.e., n > 1000) dataset would uncover more subtle relationships between absorption and the brain (Marek et al., 2022). Nonetheless, our results motivate a closer critical look at absorption as a construct, and call into question the general idea that complex personality traits can be straightforwardly associated with baseline neurobiological signatures. Future work should evaluate whether absorption is truly a stable personality trait that is uniformly expressed in individuals who score highly on the TAS/MODTAS, or whether it integrates multiple neurobiologically distinct tendencies that can be evoked in varying ways depending on context (Luhrmann et al., 2021). The differential effects across absorption subscales reported above also suggests that particular dimensions of this trait may vary in the extent to which they can be grounded in a reliable neurocognitive mechanism.

Tellegen initially proposed the TAS as the beginning – not the end – of assessments of this ostensible trait; and yet it went on to become the standard measure in the field for nearly five decades (Tellegen and Atkinson, 1974). Our finding that absorption does not reliably correlate with brain structure or function underscores the challenge of

deciphering this perplexing personality scale – a simple questionnaire that, while holding a great deal of power when it comes to predicting a range of psychological phenomena, so far seems to elude a simple mechanistic explanation. We hope that our study motivates further investigations to unravel the complex workings of this widely relevant psychological construct.

Declaration of competing interest

The authors declare that they have no known competing financial interests or personal relationships that could have appeared to influence the work reported in this paper.

Data availability

The presently used datasets are available on the OpenNeuro database.

Acknowledgements

MG acknowledges funding from National Sciences and Engineering Research Council of Canada (NSERC; Alexander Graham Bell Canada Graduate Scholarships, CGS-D). ML acknowledges funding from the Bial Foundation. The authors would like to thank Lukas Snoek for his assistance with providing the Tellegen Absorption Scale data collected in the PIOP1 dataset.

Appendix A. Supplementary data

Supplementary data to this article can be found online at https://doi.org/10.1016/j.ynirp.2023.100171.

References

Aday, J.S., Davis, A.K., Mitzkovitz, C.M., Bloesch, E.K., Davoli, C.C., 2021. Predicting reactions to psychedelic drugs: a systematic review of states and traits related to acute drug effects. ACS Pharmacology & Translational Science.
Allen, E.A., Damaraju, E., Plis, S.M., Erhardt, E.B., Eichele, T., Calhoun, V.D., 2014. Tracking whole-brain connectivity dynamics in the resting state. Cerebr. Cortex 24 (3), 663–676.
Ashburner, J., Friston, K.J., 2000. Voxel-based morphometry—the methods. Neuroimage 11 (6), 805–821.
Avants, B.B., Tustison, N., Song, G., 2009. Advanced normalization tools (ANTS). Insight j 2 (365), 1–35.
Avinun, R., Israel, S., Knodt, A.R., Hariri, A.R., 2020. Little evidence for associations between the big five personality traits and variability in brain gray or white matter. Neuroimage 220, 117092.
Balthazard, C.G., Woody, E.Z., 1992. The spectral analysis of hypnotic performance with respect to "absorption.". IJCEH (Int. J. Clin. Exp. Hypn.) 40 (1), 21–43.
Barnier, A.J., McConkey, K.M., 1999. Absorption, hypnotizability and context: non-hypnotic contexts are not all the same. Contemp. Hypn. 16 (1), 1–8.
Bassett, D.S., Sporns, O., 2017. Network neuroscience. Nat. Neurosci. 20 (3), 353–364.
Bassett, D.S., Wymbs, N.F., Porter, M.A., Mucha, P.J., Carlson, J.M., Grafton, S.T., 2011. Dynamic reconfiguration of human brain networks during learning. Proc. Natl. Acad. Sci. USA 108 (18), 7641–7646.
Behzadi, Y., Restom, K., Liau, J., Liu, T.T., 2007. A component based noise correction method (CompCor) for BOLD and perfusion based fMRI. Neuroimage 37 (1), 90–101.
Benning, S.D., Rozalski, V., Klingspon, K.L., 2015. Trait absorption is related to enhanced emotional picture processing and reduced processing of secondary acoustic probes. Psychophysiology 52 (10), 1409–1415.
Bethlehem, R.A., Paquola, C., Seidlitz, J., Ronan, L., Bernhardt, B., Tsvetanov, K.A., Consortium, C.-C., 2020. Dispersion of functional gradients across the adult lifespan. Neuroimage 222, 117299.
Blondel, V.D., Guillaume, J.-L., Lambiotte, R., Lefebvre, E., 2008. Fast unfolding of communities in large networks. J. Stat. Mech. Theor. Exp. 2008 (10), P10008.
Boekel, W., Wagenmakers, E.-J., Belay, L., Verhagen, J., Brown, S., Forstmann, B.U., 2015. A purely confirmatory replication study of structural brain-behavior correlations. Cortex 66, 115–133.
Braun, U., Schäfer, A., Bassett, D.S., Rausch, F., Schweiger, J.I., Bilek, E., Erk, S., Romanczuk-Seiferth, N., Grimm, O., Geiger, L.S., 2016. Dynamic brain network reconfiguration as a potential schizophrenia genetic risk mechanism modulated by NMDA receptor function. Proc. Natl. Acad. Sci. USA 113 (44), 12568–12573.
Braun, U., Schäfer, A., Walter, H., Erk, S., Romanczuk-Seiferth, N., Haddad, L., Schweiger, J.I., Grimm, O., Heinz, A., Tost, H., 2015. Dynamic reconfiguration of frontal brain networks during executive cognition in humans. Proc. Natl. Acad. Sci. USA 112 (37), 11678–11683.
Bresnick, T., Levin, R., 2006. Phenomenal qualities of ayahuasca ingestion and its relation to fringe consciousness and personality. J. Conscious. Stud. 13 (9), 5–24.
Buckner, R.L., Krienen, F.M., Castellanos, A., Diaz, J.C., Yeo, B.T., 2011. The organization of the human cerebellum estimated by intrinsic functional connectivity. Am. J. Physiol. Heart Circ. Physiol.
Buckner, R.L., Krienen, F.M., Yeo, B.T.T., 2013. Opportunities and limitations of intrinsic functional connectivity MRI. Nat. Neurosci. 16 (7), 832–837.
Button, K.S., Ioannidis, J.P., Mokrysz, C., Nosek, B.A., Flint, J., Robinson, E.S., Munafò, M.R., 2013. Power failure: why small sample size undermines the reliability of neuroscience. Nat. Rev. Neurosci. 14 (5), 365–376.
Cardeña, E., Terhune, D.B., 2014. Hypnotizability, personality traits, and the propensity to experience alterations of consciousness. Psychology of Consciousness: Theory, Research, and Practice 1 (3), 292.
Casey, B., Cannonier, T., Conley, M.I., Cohen, A.O., Barch, D.M., Heitzeg, M.M., Soules, M.E., Teslovich, T., Dellarco, D.V., Garavan, H., 2018. The adolescent brain cognitive development (ABCD) study: imaging acquisition across 21 sites. Developmental cognitive neuroscience 32, 43–54.
Ciric, R., Rosen, A.F., Erus, G., Cieslak, M., Adebimpe, A., Cook, P.A., Bassett, D.S., Davatzikos, C., Wolf, D.H., Satterthwaite, T.D., 2018. Mitigating head motion artifact in functional connectivity MRI. Nat. Protoc. 13 (12), 2801–2826.
Coifman, R.R., Lafon, S., Lee, A.B., Maggioni, M., Nadler, B., Warner, F., Zucker, S.W., 2005. Geometric diffusions as a tool for harmonic analysis and structure definition of data: diffusion maps. Proc. Natl. Acad. Sci. USA 102 (21), 7426–7431.
Cole, M.W., Bassett, D.S., Power, J.D., Braver, T.S., Petersen, S.E., 2014. Intrinsic and task-evoked network architectures of the human brain. Neuron 83 (1), 238–251.
Costa Jr., P.T., McCrae, R.R., 2008. The Revised Neo Personality Inventory (Neo-pi-r). Sage Publications, Inc.
Costa, P., McCrae, R., 1989. NEO Five-Factor Inventory (NEO-FFI), 3. Psychological Assessment Resources, Odessa, FL.
Cox, R.W., 1996. AFNI: software for analysis and visualization of functional magnetic resonance neuroimages. Comput. Biomed. Res. 29 (3), 162–173.
Cui, X., Ding, C., Wei, J., Xue, J., Wang, X., Wang, B., Xiang, J., 2021. Analysis of dynamic network reconfiguration in adults with attention-deficit/hyperactivity disorder based multilayer network. Cerebr. Cortex 31 (11), 4945–4957.
Damoiseaux, J., Rombouts, S., Barkhof, F., Scheltens, P., Stam, C., Smith, S.M., Beckmann, C., 2006. Consistent resting-state networks across healthy subjects. Proc. Natl. Acad. Sci. USA 103 (37), 13848–13853.
Davidson, R.J., Schwartz, G.E., Rothman, L.P., 1976. Attentional style and the self-regulation of mode-specific attention: an electroencephalograhic study. J. Abnorm. Psychol. 85 (6), 611.
Daws, R.E., Timmermann, C., Giribaldi, B., Sexton, J.D., Wall, M.B., Erritzoe, D., Roseman, L., Nutt, D., Carhart-Harris, R., 2022. Increased global integration in the brain after psilocybin therapy for depression. Nat. Med. https://doi.org/10.1038/s41591-022-01744-z.
de Wael, R.V., Benkarim, O., Paquola, C., Lariviere, S., Royer, J., Tavakol, S., Xu, T., Hong, S.-J., Langs, G., Valk, S., 2020. BrainSpace: a toolbox for the analysis of macroscale gradients in neuroimaging and connectomics datasets. Commun. biol. 3 (1), 1–10.
DeYoung, C.G., Sassenberg, T.A., Abend, R., Allen, T., Beaty, R., Bellgrove, M., Blain, S. D., Bzdok, D., Chavez, R.S., Engel, S.A., 2022. Reproducible Between-Person Brain-Behavior Associations Do Not Always Require Thousands of Individuals.
Dixon, M.L., De La Vega, A., Mills, C., Andrews-Hanna, J., Spreng, R.N., Cole, M.W., Christoff, K., 2018. Heterogeneity within the Frontoparietal Control Network and its Relationship to the Default and Dorsal Attention Networks. Proceedings of the National Academy of Sciences, 201715766.
Dong, D., Yao, D., Wang, Y., Hong, S.-J., Genon, S., Xin, F., Jung, K., He, H., Chang, X., Duan, M., 2021. Compressed sensorimotor-to-transmodal hierarchical organization in schizophrenia. Psychol. Med. 1–14.
Dubois, J., Adolphs, R., 2016. Building a science of individual differences from fMRI. Trends Cognit. Sci. 20 (6), 425–443. https://doi.org/10.1016/j.tics.2016.03.014.
Dubois, J., Galdi, P., Han, Y., Paul, L.K., Adolphs, R., 2018. Resting-state functional brain connectivity best predicts the personality dimension of openness to experience. Personality Neurosci. 1.
Esteban, O., Markiewicz, C.J., Blair, R.W., Moodie, C.A., Isik, A.I., Erramuzpe, A., Kent, J. D., Goncalves, M., DuPre, E., Snyder, M., 2019. fMRIPrep: a robust preprocessing pipeline for functional MRI. Nat. Methods 16 (1), 111–116.
Finn, E.S., Bandettini, P.A., 2021. Movie-watching outperforms rest for functional connectivity-based prediction of behavior. Neuroimage 235, 117963.
Finn, E.S., Scheinost, D., Finn, D.M., Shen, X., Papademetris, X., Constable, R.T., 2017. Can brain state be manipulated to emphasize individual differences in functional connectivity? Neuroimage 160, 140–151.
Fischl, B., 2012. FreeSurfer. *Neuroimage* 62 (2), 774–781.
Gaser, C., Dahnke, R., 2016. CAT-A Computational Anatomy Toolbox for the Analysis of Structural MRI Data. Hbm, pp. 336–348, 2016.
Genon, S., Eickhoff, S.B., Kharabian, S., 2022. Linking interindividual variability in brain structure to behaviour. Nat. Rev. Neurosci. 1–12.
Girn, M., Roseman, L., Bernhardt, B., Smallwood, J., Carhart-Harris, R., Spreng, R.N., 2021. Serotonergic psychedelic drugs LSD and psilocybin reduce the hierarchical differentiation of unimodal and transmodal cortex. bioRxiv, 072314, 2020.2005. 2001.
Glicksohn, J., Barrett, T.R., 2003. Absorption and hallucinatory experience. Appl. Cognit. Psychol.: Off. J. Soc. Appl Res. Memory Cognition 17 (7), 833–849.
Granqvist, P., Fredrikson, M., Unge, P., Hagenfeldt, A., Valind, S., Larhammar, D., Larsson, M., 2005. Sensed presence and mystical experiences are predicted by suggestibility, not by the application of transcranial weak complex magnetic fields. Neurosci. Lett. 379 (1), 1–6.

Grant, J.A., Duerden, E.G., Courtemanche, J., Cherkasova, M., Duncan, G.H., Rainville, P., 2013. Cortical thickness, mental absorption and meditative practice: possible implications for disorders of attention [Research Support, Non-U.S. Gov't]. Biol. Psychol. 92 (2), 275–281. https://doi.org/10.1016/j.biopsycho.2012.09.007.
Gratton, C., Laumann, T.O., Nielsen, A.N., Greene, D.J., Gordon, E.M., Gilmore, A.W., Nelson, S.M., Coalson, R.S., Snyder, A.Z., Schlaggar, B.L., 2018. Functional brain networks are dominated by stable group and individual factors, not cognitive or daily variation. Neuron 98 (2), 439–452 e435.
Greene, A.S., Gao, S., Scheinost, D., Constable, R.T., 2018. Task-induced brain state manipulation improves prediction of individual traits. Nat. Commun. 9 (1), 1–13.
Haak, K.V., Marquand, A.F., Beckmann, C.F., 2018. Connectopic mapping with resting-state fMRI. Neuroimage 170, 83–94.
Haijen, E.C., Kaelen, M., Roseman, L., Timmermann, C., Kettner, H., Russ, S., Nutt, D., Daws, R.E., Hampshire, A.D., Lorenz, R., 2018. Predicting responses to psychedelics: a prospective study. Front. Pharmacol. 9, 897.
Honey, C.J., Sporns, O., Cammoun, L., Gigandet, X., Thiran, J.P., Meuli, R., Hagmann, P., 2009. Predicting human resting-state functional connectivity from structural connectivity [Research Support, Non-U.S. Gov't]. Proc. Natl. Acad. Sci. U. S. A. 106 (6), 2035–2040. https://doi.org/10.1073/pnas.0811168106.
Hong, S.-J., de Wael, R.V., Bethlehem, R.A., Lariviere, S., Paquola, C., Valk, S.L., Milham, M.P., Di Martino, A., Margulies, D.S., Smallwood, J., 2019. Atypical functional connectome hierarchy in autism. Nat. Commun. 10 (1), 1022.
Huntenburg, J.M., Bazin, P.-L., Margulies, D.S., 2018. Large-scale gradients in human cortical organization. Trends Cognit. Sci. 22 (1), 21–31.
Ioannidis, J.P., 2005. Why most published research findings are false. PLoS Med. 2 (8), e124.
Ioannidis, J.P., 2008. Why most discovered true associations are inflated. Epidemiology 19 (5), 640–648.
Jamieson, G.A., 2005. The modified Tellegen absorption scale: a clearer window on the structure and meaning of absorption. Aust. J. Clin. Exp. Hypn. 33 (2), 119.
Jenkinson, M., Beckmann, C.F., Behrens, T.E., Woolrich, M.W., Smith, S.M., 2012. FSL. *Neuroimage* 62 (2), 782–790.
Kihlstrom, J.F., Register, P.A., Hoyt, I.P., Albright, J.S., Grigorian, E.M., Heindel, W.C., Morrison, C.R., 1989. Dispositional correlates of hypnosis: a phenomenological approach. IJCEH (Int. J. Clin. Exp. Hypn.) 37 (3), 249–263.
Krimmel, S.R., White, M.G., Panicker, M.H., Barrett, F.S., Mathur, B.N., Seminowicz, D. A., 2019. Resting state functional connectivity and cognitive task-related activation of the human claustrum. Neuroimage 196, 59–67.
Leonardi, N., Van De Ville, D., 2015. On spurious and real fluctuations of dynamic functional connectivity during rest. Neuroimage 104, 430–436.
Li, J., Kong, R., Liégeois, R., Orban, C., Tan, Y., Sun, N., Holmes, A.J., Sabuncu, M.R., Ge, T., Yeo, B.T., 2019. Global signal regression strengthens association between resting-state functional connectivity and behavior. Neuroimage 196, 126–141.
Lifshitz, M., van Elk, M., Luhrmann, T.M., 2019. Absorption and spiritual experience: a review of evidence and potential mechanisms. Conscious. Cognit. 73, 102760.
Luhrmann, T.M., Morgain, R., 2012. Prayer as inner sense cultivation: an attentional learning theory of spiritual experience. Ethos 40 (4), 359–389.
Luhrmann, T.M., Nusbaum, H., Thisted, R., 2010. The absorption hypothesis: learning to hear God in evangelical Christianity. Am. Anthropol. 112 (1), 66–78.
Luhrmann, T.M., Nusbaum, H., Thisted, R., 2013. Lord, teach us to pray": prayer practice affects cognitive processing. J. Cognit. Cult. 13 (1–2), 159–177.
Luhrmann, T.M., Weisman, K., Aulino, F., Brahinsky, J.D., Dulin, J.C., Dzokoto, V.A., Legare, C.H., Lifshitz, M., Ng, E., Ross-Zehnder, N., 2021. Reply to Terhune and Jamieson: the nature of absorption. Proc. Natl. Acad. Sci. USA 118 (32).
Lurie, D., Kessler, D., Bassett, D., Betzel, R.F., Breakspear, M., Keilholz, S., Kucyi, A., Liégeois, R., Lindquist, M.A., McIntosh, A.R., 2018. On the nature of resting fMRI and time-varying functional connectivity. PsyArXiv Preprints.
Maij, D.L., van Elk, M., 2018. Getting absorbed in experimentally induced extraordinary experiences: effects of placebo brain stimulation on agency detection. Conscious. Cognit. 66, 1–16.
Manmiller, J.L., Kumar, V., Pekala, R.J., 2005. Hypnotizability, creative capacity, creativity styles, absorption, and phenomenological experience during hypnosis. Creativ. Res. J. 17 (1), 9–24.
Marek, S., Tervo-Clemmens, B., Calabro, F.J., Montez, D.F., Kay, B.P., Hatoum, A.S., Donohue, M.R., Foran, W., Miller, R.L., Hendrickson, T.J., 2022. Reproducible brain-wide association studies require thousands of individuals. Nature 603 (7902), 654–660.
Margulies, D.S., Ghosh, S.S., Goulas, A., Falkiewicz, M., Huntenburg, J.M., Langs, G., Bezgin, G., Eickhoff, S.B., Castellanos, F.X., Petrides, M., 2016. Situating the default-mode network along a principal gradient of macroscale cortical organization. Proc. Natl. Acad. Sci. USA 113 (44), 12574–12579.
Masouleh, S.K., Eickhoff, S.B., Hoffstaedter, F., Genon, S., Initiative, A.s.D.N., 2019. Empirical examination of the replicability of associations between brain structure and psychological variables. Elife 8, e43464.
McConkey, K.M., Wende, V., Barnier, A.J., 1999. Measuring change in the subjective experience of hypnosis. IJCEH (Int. J. Clin. Exp. Hypn.) 47 (1), 23–39.
McCrae, R.R., 1993. Openness to experience as a basic dimension of personality. Imagin., Cognit. Pers. 13 (1), 39–55.
McCrae, R.R., Costa Jr., P.T., 1985. Openness to experience. Perspectives in personality 1, 145–172.
McIntosh, A.R., Lobaugh, N.J., 2004. Partial least squares analysis of neuroimaging data: applications and advances. Neuroimage 23, S250–S263.
McIntosh, A.R., Mišić, B., 2013. Multivariate statistical analyses for neuroimaging data. Annu. Rev. Psychol. 64, 499–525.
Mendes, N., Oligschlaeger, S., Lauckner, M.E., Golchert, J., Huntenburg, J.M., Falkiewicz, M., Ellamil, M., Krause, S., Baczkowski, B.M., Cozatl, R., 2019. A functional connectome phenotyping dataset including cognitive state and personality measures. Sci. Data 6, 180307.
Mucha, P.J., Richardson, T., Macon, K., Porter, M.A., Onnela, J.-P., 2010. Community structure in time-dependent, multiscale, and multiplex networks. Science 328 (5980), 876–878.
Murphy, C., Jefferies, E., Rueschemeyer, S.-A., Sormaz, M., Wang, H.-t., Margulies, D.S., Smallwood, J., 2018. Distant from input: evidence of regions within the default mode network supporting perceptually-decoupled and conceptually-guided cognition. Neuroimage 171, 393–401.
Murphy, K., Fox, M.D., 2017. Towards a consensus regarding global signal regression for resting state functional connectivity MRI. Neuroimage 154, 169–173.
Newman, M.E., 2004. Fast algorithm for detecting community structure in networks. Phys. Rev. 69 (6), 066133.
Ott, U., 2007. States of Absorption: in Search of Neurobiological Foundations. *Hypnosis And Conscious States: The Cognitive Neuroscience Perspective*, pp. 257–270.
Ott, U., Reuter, M., Hennig, J., Vaitl, D., 2005. Evidence for a common biological basis of the absorption trait, hallucinogen effects, and positive symptoms: epistasis between 5-HT2a and COMT polymorphisms. Am. J. Med. Genet. Part B: Neuropsychiatric Genetics 137 (1), 29–32.
Paquola, C., De Wael, R.V., Wagstyl, K., Bethlehem, R.A., Hong, S.-J., Seidlitz, J., Bullmore, E.T., Evans, A.C., Misic, B., Margulies, D.S., 2019. Microstructural and functional gradients are increasingly dissociated in transmodal cortices. PLoS Biol. 17 (5), e3000284.
Paquola, C., Seidlitz, J., Benkarim, O., Royer, J., Klimes, P., Bethlehem, R.A., Lariviere, S., de Wael, R.V., Hall, J.A., Frauscher, B., 2020. The Cortical Wiring Scheme of Hierarchical Information Processing. bioRxiv.
Perona-Garcelán, S., Bellido-Zanin, G., Rodríguez-Testal, J.F., López-Jiménez, A.M., García-Montes, J.M., Ruiz-Veguilla, M., 2016. The relationship of depersonalization and absorption to hallucinations in psychotic and non-clinical participants. Psychiatr. Res. 244, 357–362.
Perona-Garcelán, S., García-Montes, J.M., Rodríguez-Testal, J.F., Ruiz-Veguilla, M., Benítez-Hernández, M.d.M., López-Jiménez, A.M., Arias-Velarde, M.Á., Ductor-Recuerda, M.J., Gómez-Gómez, M.T., Pérez-Álvarez, M., 2013. Relationship of absorption, depersonalisation, and self-focused attention in subjects with and without hallucination proneness. Cognit. Neuropsychiatry 18 (5), 422–436.
Poldrack, R.A., Baker, C.I., Durnez, J., Gorgolewski, K.J., Matthews, P.M., Munafò, M.R., Nichols, T.E., Poline, J.-B., Vul, E., Yarkoni, T., 2017. Scanning the horizon: towards transparent and reproducible neuroimaging research. Nat. Rev. Neurosci. 18 (2), 115–126.
Power, J.D., Barnes, K.A., Snyder, A.Z., Schlaggar, B.L., Petersen, S.E., 2012. Spurious but systematic correlations in functional connectivity MRI networks arise from subject motion. Neuroimage 59 (3), 2142–2154.
Power, J.D., Mitra, A., Laumann, T.O., Snyder, A.Z., Schlaggar, B.L., Petersen, S.E., 2014. Methods to detect, characterize, and remove motion artifact in resting state fMRI. Neuroimage 84, 320–341.
Raichle, M.E., 2009. A paradigm shift in functional brain imaging. J. Neurosci. 29 (41), 12729–12734. https://doi.org/10.1523/jneurosci.4366-09.2009.
Rubinov, M., Sporns, O., 2010. Complex network measures of brain connectivity: uses and interpretations. Neuroimage 52 (3), 1059–1069.
Schaefer, A., Kong, R., Gordon, E.M., Laumann, T.O., Zuo, X.-N., Holmes, A.J., Eickhoff, S.B., Yeo, B., 2017. Local-global parcellation of the human cerebral cortex from intrinsic functional connectivity mri. Cerebr. Cortex 1–20.
Setton, R., Mwilambwe-Tshilobo, L., Girn, M., Lockrow, A.W., Baracchini, G., Lowe, A.J., Cassidy, B.N., Li, J., Luh, W.-M., Bzdok, D., Leahy, R.M., Ge, T., Margulies, D.S., Misic, B., Bernhardt, B.C., Dale Stevens, W., Brigard, F.D., Kundu, P., Turner, G.R., Nathan Spreng, R., 2021. Functional Architecture of the Aging Brain. bioRxiv. https://doi.org/10.1101/2021.03.31.437922, 2021.2003.2031.437922.
Shafiei, G., Zeighami, Y., Clark, C.A., Coull, J.T., Nagano-Saito, A., Leyton, M., Dagher, A., Mišić, B., 2019. Dopamine signaling modulates the stability and integration of intrinsic brain networks. Cerebr. Cortex 29 (1), 397–409.
Smallwood, J., Bernhardt, B.C., Leech, R., Bzdok, D., Jefferies, E., Margulies, D.S., 2021. The default mode network in cognition: a topographical perspective. Nat. Rev. Neurosci. 1–11.
Smith, S.M., Fox, P.T., Miller, K.L., Glahn, D.C., Fox, P.M., Mackay, C.E., Filippini, N., Watkins, K.E., Toro, R., Laird, A.R., 2009. Correspondence of the brain's functional architecture during activation and rest. Proc. Natl. Acad. Sci. USA 106 (31), 13040–13045.
Smith, S.M., Nichols, T.E., Vidaurre, D., Winkler, A.M., Behrens, T.E., Glasser, M.F., Ugurbil, K., Barch, D.M., Van Essen, D.C., Miller, K.L., 2015. A positive-negative mode of population covariation links brain connectivity, demographics and behavior. Nat. Neurosci. 18 (11), 1565.
Snoek, L., van der Miesen, M.M., Beemsterboer, T., van der Leij, A., Eigenhuis, A., Steven Scholte, H., 2021. The Amsterdam Open MRI Collection, a set of multimodal MRI datasets for individual difference analyses. Sci. Data 8 (1), 1–23.
Spreng, R.N., Stevens, W.D., Chamberlain, J.P., Gilmore, A.W., Schacter, D.L., 2010. Default network activity, coupled with the frontoparietal control network, supports goal-directed cognition [Research Support, N.I.H., Extramural]. Neuroimage 53 (1), 303–317. https://doi.org/10.1016/j.neuroimage.2010.06.016.
Stevens, W.D., Spreng, R.N., 2014. Resting-state functional connectivity MRI reveals active processes central to cognition. Wiley Interdisciplinary Reviews: Cognit. Sci. 5 (2), 233–245.
Studerus, E., Gamma, A., Kometer, M., Vollenweider, F.X., 2012. Prediction of psilocybin response in healthy volunteers. PLoS One 7 (2).
Sudlow, C., Gallacher, J., Allen, N., Beral, V., Burton, P., Danesh, J., Downey, P., Elliott, P., Green, J., Landray, M., 2015. UK biobank: an open access resource for

identifying the causes of a wide range of complex diseases of middle and old age. PLoS Med. 12 (3), e1001779.
Sutcliffe, J., Perry, C., Sheehan, P.W., 1970. Relation of some aspects of imagery and fantasy to hypnotic susceptibility. J. Abnorm. Psychol. 76 (2), 279.
Sydnor, V.J., Larsen, B., Bassett, D.S., Alexander-Bloch, A., Fair, D.A., Liston, C., Mackey, A.P., Milham, M.P., Pines, A., Roalf, D.R., 2021. Neurodevelopment of the association cortices: patterns, mechanisms, and implications for psychopathology. Neuron 109 (18), 2820–2846.
Tagliazucchi, E., Roseman, L., Kaelen, M., Orban, C., Muthukumaraswamy, S.D., Murphy, K., Laufs, H., Leech, R., McGonigle, J., Crossley, N., 2016. Increased global functional connectivity correlates with LSD-Induced ego dissolution. Curr. Biol. 26 (8), 1043–1050.
Tellegen, A., 1981. Practicing the Two Disciplines for Relaxation and Enlightenment: Comment on" Role of the Feedback Signal in Electromyograph Biofeedback: the Relevance of Attention" by Qualls and Sheehan.
Tellegen, A., 1982. *Unpublished manuscript*. Brief Manual for the Multidimensional Personality Questionnaire, 8. University of Minnesota, Minneapolis, 1031-1010.
Tellegen, A., Atkinson, G., 1974. Openness to absorbing and self-altering experiences (" absorption"), a trait related to hypnotic susceptibility. J. Abnorm. Psychol. 83 (3), 268.
Terhune, D.B., Jamieson, G.A., 2021. Hallucinations and the meaning and structure of absorption. Proc. Natl. Acad. Sci. USA 118 (32), e2108467118.
Terhune, D.B., Luke, D.P., Kaelen, M., Bolstridge, M., Feilding, A., Nutt, D., Carhart-Harris, R., Ward, J., 2016. A placebo-controlled investigation of synaesthesia-like experiences under LSD. Neuropsychologia 88, 28–34.
Tian, Y., Margulies, D.S., Breakspear, M., Zalesky, A., 2020. Topographic organization of the human subcortex unveiled with functional connectivity gradients. Nat. Neurosci. 23 (11), 1421–1432.
Tiego, J., Fornito, A., 2022. Putting Behaviour Back into Brain-Behaviour Correlation Analyses.
Timmermann, C., Roseman, L., Williams, L., Erritzoe, D., Martial, C., Cassol, H., Laureys, S., Nutt, D., Carhart-Harris, R., 2018. DMT models the near-death experience. Front. Psychol. 1424.
Van Dijk, K.R., Hedden, T., Venkataraman, A., Evans, K.C., Lazar, S.W., Buckner, R.L., 2010. Intrinsic functional connectivity as a tool for human connectomics: theory, properties, and optimization. J. Neurophysiol. 103 (1), 297.
Van Essen, D.C., Smith, S.M., Barch, D.M., Behrens, T.E., Yacoub, E., Ugurbil, K., Consortium, W.-M.H., 2013. The Wu-Minn human connectome project: an overview. Neuroimage 80, 62–79.
Vartanian, O., Wertz, C.J., Flores, R.A., Beatty, E.L., Smith, I., Blackler, K., Lam, Q., Jung, R.E., 2018. Structural correlates of Openness and Intellect: implications for the contribution of personality to creativity. Hum. Brain Mapp. 39 (7), 2987–2996.
Vázquez-Rodríguez, B., Suárez, L.E., Markello, R.D., Shafiei, G., Paquola, C., Hagmann, P., Van Den Heuvel, M.P., Bernhardt, B.C., Spreng, R.N., Misic, B., 2019. Gradients of structure–function tethering across neocortex. Proc. Natl. Acad. Sci. USA 116 (42), 21219–21227.
Wickramasekera, I.E., 2007. Empathic features of absorption and incongruence. Am. J. Clin. Hypn. 50 (1), 59–69.
Wickramasekera, I.E., Szlyk, J.P., 2003. Could empathy be a predictor of hypnotic ability? IJCEH (Int. J. Clin. Exp. Hypn.) 51 (4), 390–399.
Wild, T.C., Kuiken, D., Schopflocher, D., 1995. The role of absorption in experiential involvement. J. Pers. Soc. Psychol. 69 (3), 569.
Xia, M., Wang, J., He, Y., 2013. BrainNet Viewer: a network visualization tool for human brain connectomics. PLoS One 8 (7), e68910.
Yeo, B.T.T., Kirienen, F.M., Sepulcre, J., Sabuncu, M.R., Lashkari, D., Hollinshead, M., Roffman, J.L., Smoller, J.W., Zöllei, L., Polimeni, J.R., Fischl, B., Liu, H., Buckner, R. L., 2011. The organization of the human cerebral cortex estimated by intrinsic functional connectivity. J. Neurophysiol. 106, 1125–1165. https://doi.org/10.1152/jn.00338.2011.
Yin, W., Li, T., Hung, S.-C., Zhang, H., Wang, L., Shen, D., Zhu, H., Mucha, P.J., Cohen, J. R., Lin, W., 2020. The emergence of a functionally flexible brain during early infancy. Proc. Natl. Acad. Sci. USA 117 (38), 23904–23913.
Yin, W., Li, T., Mucha, P.J., Cohen, J.R., Zhu, H., Zhu, Z., Lin, W., 2022. Altered neural flexibility in children with attention-deficit/hyperactivity disorder. Mol. Psychiatr. 1–7.
Zuo, X.-N., Kelly, C., Adelstein, J.S., Klein, D.F., Castellanos, F.X., Milham, M.P., 2010. Reliable intrinsic connectivity networks: test–retest evaluation using ICA and dual regression approach. Neuroimage 49 (3), 2163–2177.